Master's thesis

# Concentration profiles of ferrofluids in magnetic fields

## Thermodynamic theory and analytical centrifugation

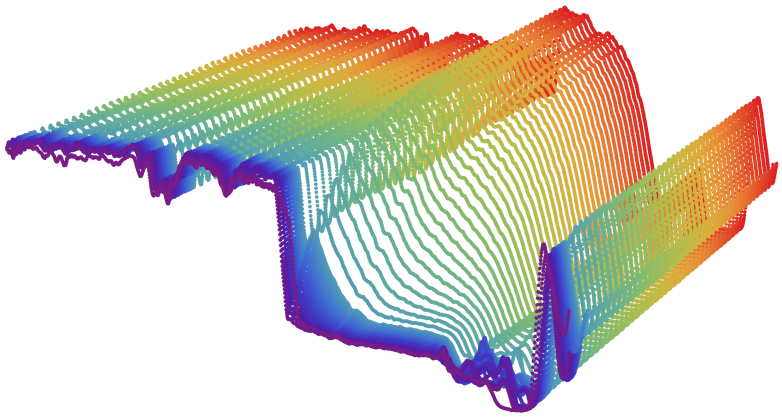


Utrecht University

Physical & colloid chemistry

*Author:*
Willem Boon

*Supervisors:*
Alex van Silfhout
Ben Erné


February 28, 2018

**Abstract**

Ferrofluids are dispersion of magnetic nanoparticles which are often used in magnetic field gradients during applications. When the magnetic field gradient is sufficiently strong it can pull magnetic nanoparticles out of solution, an unwanted side effect often described through theory based on ideal point dipoles. In this thesis, a closed form equation for the concentration profile of point dipoles in arbitrary fields is derived. It is found that for magnets much smaller than the fluid column, the concentration of nanoparticles near the magnet exceeds the densest packing fraction. For a better description, concentration profiles accounting for the excluded volume of particles are described with thermodynamic theory. Furthermore, an original theory describing the timescale of the sedimentation towards an equilibrium concentration profile is derived. This theory does not try to solve the full concentration profile as function of time, but rather it describes the flux through a point that starts at the equilibrium concentration. The advantage of this theory is that it can describe the sedimentation of particles with interactions in arbitrary fields.

These new theories were used to describe new, original measurements of concentration profiles in magnetized ferrofluids in an analytical centrifuge. The equilibrium theory accounting for excluded volume fits the measured profiles much better than the theory assuming point dipoles. The time-dependent theory matches the experiments reasonably well, both in timescale and average concentration change, with an improvement of two orders of magnitude over a previously reported method [Taketome, Jap.J.Appl.Phys., 1980].

# Contents

# 1 Introduction

Ferrofluids are dispersions of magnetic nanoparticles in a carrier liquid. Within this liquid, particles move freely through Brownian motion. Consequently, the particles spread out across the system. As the particles are magnetizable, the fluid effectively becomes a liquid magnet [1]. By applying a magnetic field to the ferrofluid interesting physical phenomena can be realized. For instance, the attraction of the fluid to a magnet can be used to magnetically levitate heavier objects in the fluid [2, 3]. Another, common, application is the use of ferrofluids for rotary pressure seals [4]. More subtle effects, like the interaction between fluid instabilities and geometrically constrained magnetic flux, can give rise to beautiful geometrical patterns[5]. Most, but not all, of these interesting effects are realized when a magnetic field gradient is applied to the ferrofluid.

While the magnetic field gradient is the driving force in these phenomena, a magnetic field gradient will also pull on the magnetic particles. When the force is large enough, the particles will be pulled out of the fluid, lowering the magnetization in the bulk of the fluid and increasing near the magnet[1, 4, 6, 7]. This is often an unwanted side effect. In this master's thesis the effect of demagnetization by an applied magnetic field gradient will be studied. We will study this by analytical centrifugation in the presence of a magnet, thereby measuring concentration profiles of magnetized ferrofluids.

In Chapter 2 we will give a general overview of the theoretical concepts that will be used in this thesis. The topics that will be covered are classical thermodynamics, magnetic dipoles and diffusion equations. In Chapter 3 we will present original thermodynamic theory on the concentration profiles of magnetic dipoles in magnetic fields. Topics that will be covered are concentration profiles in linear and non-linear fields and the effect of excluded volume interactions. In Chapter 4 we will present a new way to use Fick's law of diffusion to calculate a time scale for the sedimentation process. In Chapter 5 we will present experimental work for the direct characterization of concentration profiles by analytical centrifugation. In Chapter 6 the results of these experiments are shown and compared to the presented theory.

# 2 Introductory theory

## 2.1 Magnetic dipoles

A defining characteristic of magnetic nanoparticles is that they have a permanent magnetic dipole. This dipole is obtained from the alignment of the atomic dipoles in the (ferromagnetic) material. When a magnetic field is applied to a magnetic dipole, the dipole has a preferred alignment along this magnetic field, as the energy is minimized in this configuration. The energy $E$ is given by:

$$E = -\mu_0 \vec{H}\vec{m} = -\mu_0 H m \cos(\theta) \tag{1}$$

here $m$ is the magnetic dipole moment in [$\mathrm{Am}^2$], $H$ is the applied magnetic field in [$\mathrm{Am}^{-1}$], $\mu_0$ is the magnetic permeability of vacuum $4\pi \cdot 10^{-7}$[$\mathrm{JA}^{-2}\mathrm{m}^{-1}$] and $\theta$ is the angle between the dipole and the magnetic field. As magnetic nanoparticles smaller than 10 nm often have only one magnetic domain, the magnitude of a magnetic dipole can be found by simply multiplying the volume magnetization $M_s$ by the volume of the magnetic domain in the nanoparticle. The Boltzmann averaged orientation of a magnetic dipole in external field is described by the Langevin function[8], as will be described in the following section.

## 2.2 Langevin function

The Langevin function is a function that describes the expected orientation of a Brownian rotating dipole in a magnetic field. As the force on a particle is determined by the orientation of the dipole in a magnetic field, this equation will be of fundamental importance in this thesis. The orientation is determined by a competition between the kinetic energy and entropy of a particle in a magnetic field. In the high temperature limit there will be no preferred direction for the dipole orientation, while in the strong field limit the particle will be orientated in the magnetic field direction. The Langevin function is given by:

$$L(\zeta H) = \coth(\zeta H) - \frac{1}{\zeta H} \tag{2}$$

here $\zeta = \frac{\mu_0 m}{k_B T}$ in $[\mathrm{mA}^{-1}]$, $k_B$ is the Boltzmann constant given by $1.38 \cdot 10^{-23}[\mathrm{JK}^{-1}]$ and $T$ is the temperature in [K]. The function is derived by taking the Boltzmann weighted average of the dipole orientations. The function goes from $-1$ to 1, where 1 indicates that the particles are fully aligned with the field, while $-1$ indicates that the dipoles are perfectly aligned with the field in the negative direction. If the field is aligned along the $x$-axis, multiplying the magnetic dipole moment $m$ by the Langevin function one obtains $\langle m_x \rangle$, the expected magnetic moment of a particle along the magnetic field. Here the $\langle brackets \rangle$ denote the expectation value. The expected force $\langle F_m \rangle$ on a Brownian rotating magnetic dipole is then given by:

$$\langle F_m \rangle = L(\zeta H)\mu_0 m \frac{dH_x}{dx} \tag{3}$$

In the thesis the brackets will be often omitted. It can be seen that the force on a particle is determined by both the absolute value of the magnetic field and the magnetic field gradient.

## 2.3 Particle interactions

The simplest thermodynamic model system, the ideal gas, assumes that particles in the gas can be represented by point particles with no interactions. This assumption is valid for very dilute systems as the average interparticle distance is very large for these systems[9]. However, when the concentration of the system increases, particle interactions become more common as the interparticle distance decreases. The first correction that becomes significant is the two particle interaction. This is because it is more likely for two particles to be close enough to each other for significant interaction to occur, than for two particles and a third particle being close to each other. The effect of these $n$-body corrections on the thermodynamic variables is described through virial coefficients.

### 2.3.1 Virial coefficients

As the particles in an ideal gas are assumed to have no interactions, the free energy of an ideal gas is only described by the kinetic properties of the gas, and it is independent of the positions and order of the particles. The Helmholtz free energy for an ideal gas [10] is given by:

$$F_{id} = c\ln(\gamma c) - c \tag{4}$$

where $F$ is the Helmholtz free energy and $\gamma$ is a constant determined by the smallest relevant size in the system. The so called *excess* free energy, accounting for the free energy from particle interactions is independent from the kinetic, ideal gas, free energy[11]. Therefore the overall free energy is given by:

$$F = F_{id} + F_{exc} \tag{5}$$

The excess free energy accounts for all the interactions between all the particles in the system. As this is a many body system, the calculation of the full excess free energy is often not tractable. A noticeable exception is the Carnahan-Starling free energy, which describes the full excess free energy for particles with hard sphere interactions. The problem is simplified by sorting the excess free energy into the $n$-particle interactions of which it is composed. This can be done because the sum of all $n$-particle interactions accounts for all the particle interactions between all the particles. The expression for the excess free energy then reads:

$$F_{exc} = \sum_{n=2}^{\infty} \frac{B_n}{n-1} c^n \tag{6}$$

Here $B_n$ is the $n$th virial coefficient, describing a $n$-particle interaction. The denominator accounts for double counting of interactions, while the concentration the concentration $c$ to the power $n$ accounts for the chance of an $n$-particle interaction occurring. This last term also ensure that higher virial coefficients can be neglected at low concentrations. The values of the virial coefficients depend on the particle interactions that are described. The virial coefficient is negative when

attractive interactions dominate and positive when repulsive interactions dominate.

In this thesis we will often refer to hard sphere interactions. Hard sphere interactions are a way of modelling the fact that real particles cannot overlap, and therefore exclude volume. The closed form expression of $F_{exc}$ is called an equation of state, which is known for hard sphere interactions. This is the Carnahan-Starling equation of state, which will be discussed in section 3.4.

## 2.4 Fick's laws and diffusion

Fick's laws are laws that describe the tendency of particles to move from areas of high concentration to areas of low concentration [9]. The driving force for this movement is a chemical potential gradient. Fick's first law reads[11, 12]:

$$J = -\frac{Dc(x)}{k_B T}\frac{d\mu(c(x))}{dx} \tag{7}$$

here $J$ is the flux of particles in $[\mathrm{m}^{-2}\mathrm{s}^{-1}]$, $D$ is the diffusion constant in $[\mathrm{m}^2\mathrm{s}^{-1}]$, $\mu$ is the chemical potential in [J] and $c$ is the concentration in $[\mathrm{m}^{-3}]$. For the ideal chemical potential $\mu_{id} = k_B T \ln(c)$ Fick's first law reads:

$$J = -D\frac{dc}{dx} \tag{8}$$

This is the form in which Fick's first law is commonly encountered. From Fick's first law one can derive Fick's second law by assuming conservation of particles and no presence of advective flow. From conservation of particles [9] one finds:

$$\frac{\partial c}{\partial t} = -\frac{\partial}{\partial x}J \tag{9}$$

Then by simply substituting the ideal expression for Fick's first law (Eq.8) for $J$ one finds the commonly used expression for Fick's second law:

$$\frac{\partial c}{\partial t} = D\frac{\partial^2 c}{\partial x^2} \tag{10}$$

When the addition of flux by (magnetic) body forces on the particles ($J = vc(x,t)$, where $v$ is the speed) is taken into account in this derivation one finds the so called diffusion-drift or Fokker-Planck equation. For non-ideal chemical potentials this reads:

$$\frac{\partial c}{\partial t} = \frac{\partial}{\partial x}\left(\frac{Dc(x)}{kT}\frac{\partial \mu(c(x))}{\partial x} - vc(x,t)\right) \tag{11}$$

From this equation it is easily seen that in equilibrium ($\frac{\partial c}{\partial t} = 0$) diffusion counteracts the flux from body forces from external fields.

# 3 Equilibrium description

Over large time scales, a suspension of magnetic particles will settle into an equilibrium concentration profile. In equilibrium diffusion cancels out forces on particles. The definition of thermodynamic equilibrium requires that there is constant chemical potential, pressure and temperature. Using thermodynamical tools, the equilibrium concentration profile can be calculated. As this equilibrium concentration profile determines the final magnetization of the ferrofluid, this is of fundamental interest for applications. [2, 3, 5, 4, 13]

As a starting point for the analysis of the concentration profile in a ferrofluid, the nanoparticles will be treated as ideal point particles with no interparticle interactions. For simplicity, the calculations will be done for one dimensional concentration profiles. This one dimensional description is valid for real experiments if the experimental setup is approximately translationally independent in the other two dimension. The concentration profiles are calculated using the requirement of constant chemical potential at every posititon. This approach is analogues to the derivation of the barometric concentration profile as can be found in [9]. This approach was chosen over the often used pressure based description, as both the alignment of magnetic moments and non-linear fields complicate this description. The reason for this

is that in the pressure description, the total pressure at the bottom of the vessel is assumed known from initial conditions, and this is then used the calculate the concentration profile[14]. However, for magnetic particles the force on a particle depends on its position in the magnetic field and thus the total pressure at the bottom of the vessel depends on the unknown concentration profile. The final goal of the presented theory is to calculate an equilibrium concentration profile for a given magnetic field and initial concentration.

## 3.1 Point dipoles in external field

Calculation of the concentration profile starts by decomposing the chemical potential of magnetic nanoparticles into an external field potential, consisting of the potential energy of a particle in the field, and an internal thermodynamic potential [9, 10].

$$\mu(c(x), x) = \mu_{\text{int}}(c(x)) + \mu_{\text{ext}}(x) = \text{constant} \tag{12}$$

Here $\mu$ is the chemical potential, $c(x)$ is the concentration as function of position and $x$ is the position. The sum of these two chemical potentials has to be equal at every $x$ coordinate to meet the requirement of equal chemical potential.

$$\mu_{int}(c(x_1)) + \mu_{\text{ext}}(x_1) = \mu_{int}(c(x_2)) + \mu_{ext}(x_2) \tag{13}$$

This relation dictates the ratio between $c(x_1)$ and $c(x_2)$. We will define $c(x_2)$ as the reference concentration value. Sometimes an analytical function for $c(x)$ can be derived, this depends on the functions chosen for $\mu_{int}(c(x))$ and $\mu_{ext}(x)$. For a collection of ideal particles the internal chemical potential has the form of:

$$\mu_{int}(c) = \mu_0 + k_B T \ln(c) \tag{14}$$

The external potential depends on the external magnetic field. It describes the potential energy of a particle in this field at position $x$. The potential energy is defined by the work (force times distance) that a particle does when falling from position $x$ to 0, the bottom of the

vessel.

$$\mu_{ext}(x) = -\int_x^0 F_m(x')dx' \tag{15}$$

where $F_m$ is the magnetic force on a particle at position $x$. Here $x'$ is a dummy integration variable. As seen in the introduction the force of a Brownian magnetic dipole in a magnetic field gradient scales with the Langevin function. It depends on the magnetic field, temperature and magnetic field gradient. It will be useful to define the magnetic dipole moment times the magnetic permeability in a shorthand notation for future use, with $\lambda = m\mu_0 = \zeta k_B T$. The body force on a magnetic particle is the product of the orientation of the magnetic moment, given by the Langevin function [6], the magnetic field gradient and the magnetic dipole moment.

$$F_m(x) = \lambda L(\zeta H(x))\frac{dH(x)}{dx} \tag{16}$$

For ideal particles all functions needed to calculate the equilibrium profile are now known. Combining 13, 14, 15 and 16 and setting $\mu(x_1)$ to 0 we find:

$$k_B T \ln(\frac{c(x)}{c(0)}) = -\int_x^0 F_m(x')dx' \tag{17}$$

Solving for $c(x_1)$ gives:

$$c(x) = c_0 \exp(\frac{-\int_x^0 F_m(x')dx'}{k_B T}) \tag{18}$$

The integral can be solved for a specific field to give an equilibrium concentration profile for that field. Here we choose to solve it for a general field $H(x)$, because it results in a neat closed form solution of the concentration as function of field strength. Substituting Eq.3 into Eq.18 will result in the following integral:

$$\lambda \int_{H(x=0)}^{H(x)} (\coth(\zeta H) - \frac{1}{\zeta H})dH = \tag{19}$$

$$\frac{\lambda}{\zeta}(\ln(\frac{\sinh(\zeta H(x))}{H(x)}) - \ln(\frac{\sinh(\zeta H(0))}{H(0)}) \tag{20}$$

Substituting this into Eq.18 the $k_BT$ and $\frac{\lambda}{\zeta}$ terms cancel. The logarithmic and exponential terms also cancel. Defining the reference magnetization at the bottom of the sedimentation vessel as $H(0) \equiv H_0$, the final relation for ideal particles, between the concentration at the bottom ($c(x = 0) \equiv c_0$) and elevation $x$ in the ferrofluid is found.

$$c(x) = c_0 \frac{H_0 \cdot \sinh(\zeta H(x))}{H(x) \cdot \sinh(\zeta H_0)} \tag{21}$$

This result indicates that the concentration profile is purely a function of field strength, and is independent of the spatial form that the magnetic field takes. This function is equal to the description derived in [7], where it was found through the diffusion-drift equation. Thus this formula can be used to analyze the concentration profiles of ideal point dipoles for arbitrary magnetic fields. The analysis can be done in terms of position by substituting the magnetic field of interest $H(x)$ or in general terms of magnetic field strength. In Fig.1 the logarithmic plot of the reduced concentration $(c(x)/c_0)$ against field strength for particles with $\zeta = 4.5 \cdot 10^{-5}$ [m/A], corresponding to 10 nm particles at room temperature, can be seen. The initial field strength used was $H_0 = 795774$[A/m].

### 3.1.1 Densest packing fraction

The resulting concentration profile is extremely steep. To test how realistic the prediction for ideal particles is, two boundary conditions that every physical system must obey can be applied. The first boundary condition is conservation of the initial number of particles and the second is the closest sphere packing. While the thermodynamic theory used for the calculation assumes the particles have no volume, the volume occupation of the final concentration profile can be calculated straightforwardly by multiplying the number of particles by the volume of a single particle. If conservation of particles can not be met without staying under the densest sphere packing, the prediction can be said to be unphysical for that initial number of particles. Written

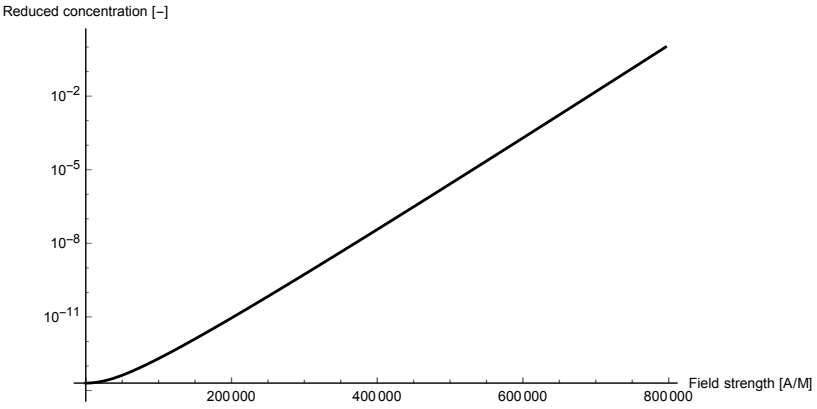


**Figure 1:** Logarithmic plot of the reduced concentration as function of field strength. The reduced concentration is defined by $c(x)/c_0$.

in mathematical form [15]:

$$\text{Densest spherepacking}: \qquad c_0 \leq \frac{\sqrt{2}}{d^3} \tag{22}$$

$$\text{Conservation of particles}: \qquad Lc_i = c_0 \int_0^L \frac{H_0 \cdot \sinh(\zeta H(x))}{H(x) \cdot \sinh(\zeta H_0)} dx \tag{23}$$

Combining these two boundary conditions results in an expression for $c_{i.max}$, the maximum initial concentration for which the ideal description gives physical predictions.

$$c_{i.max} = \frac{\sqrt{2} H_0}{d^3 L \sinh(\zeta H_0)} \int_0^L \frac{\sinh(\zeta H(x))}{H(x)} dx \tag{24}$$

This maximum concentration is system dependent, as it depends both on the system size and form of the magnetic field, and because of this, a magnetic field and sedimentation vessel geometry must be assumed. For this calculation, a literature experiment is used from Berret et al. [6]. In the experiment 10 nm magnetite particles were allowed to sediment in a constant magnetic field gradient of 10 T/m.

The experiment uses a sedimentation vessel with a length of 2 mm. Particle properties are the same as in previous calculations, giving $\zeta = 4.5 \cdot 10^{-5}$[m/A] and $H_0 = 795774$[A/m]. The resulting maximum concentration as function of system size is plotted in Fig.2.

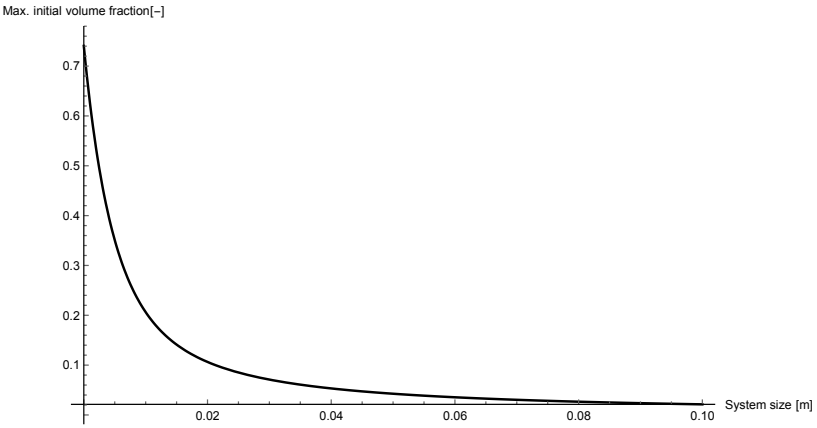


**Figure 2:** Maximum initial volume fraction for which the description of magnetic nanoparticles as point dipoles gives a physical prediction as function of system length. At a length of 10 centimeters the magnetic field has completely decayed. Note that in the limit of zero system size the maximum initial concentration equals the densest packing density.

A maximum concentration of 53 volume percent is found. This is an extremely high concentration for ferrofluids used in applications. The concentrations used in the experiments by Berret are more than an order of magnitude lower, indicating that an ideal approach is valid. By extending the sedimentation vessel length to 10 cm, the length over which the magnetic field has completely decayed, a maximum concentration of only 2.1 volume percent is found. This is a common concentration in experimental conditions, and is close to the actual experimental concentration of 2 volume percent. The ideal concentration profile is unphysical for these conditions. The linear assumption for the magnetic field is no longer valid for this system size, and in the following section we will calculate profiles for realistic non-linear fields.

### 3.1.2 Small magnets and non-linear fields

The calculation was repeated with the non-linear field of a rectangular block magnet with length ratios of $1 \times 1 \times 1$ and a remanent magnetization of $H_0 = 795774$ [A/m]. This magnet has a reference magnetization of $H_0 = 346882$[A/m] at the bottom of the sedimentation vessel. The sedimentation vessel length was kept constant at 2 cm and was aligned along the axis of magnetization of the magnet. The volume of the magnet was varied while the proportions were kept constant. The fields for large magnets decay slowly and are spread out over the entire length of the sedimentation vessel or beyond, while smaller magnets have a more localized, non-linear magnetic field that decays over a fraction of the sedimentation vessel length. Note that the energy for a magnetic particle sedimenting from 0 field to the surface of the magnet is independent of the magnet size, and only the length over which the magnetic field decays changes. The plot of the maximum initial volume fraction against magnet size can be seen in Fig.3. It is found that the maximum initial volume fraction for which the theory has physical predictions tends to 0 in the limit of small magnet sizes. This can be understood by considering that when a magnetic field decays twice as fast, the entire concentration profile is compressed by a factor two. For a magnet of $1\text{cm}^3$ the maximum initial concentration is 1.4 volume percent, again a reasonable value found in typical applications[1], results in unphysical predictions. This small magnet limit for which the ideal description is invalid is unique to ferrofluids. In the limit of an infinitely large magnet the maximum initial volume fraction equals the densest sphere packing as expected, as there is no magnetic field gradient for large magnets.

**Discussion** In the previous section the concentration profile for ideal magnetic dipoles in an external magnetic field was derived. For these concentration profiles the condition of physical packing fraction was tested for realistic linear and non-linear magnetic fields. It was found that when the magnetic field from a neodymium magnet decayed in approximately the sedimentation vessel length, the ideal concentration profiles became unphysical for realistic application concentrations. This was only a check for the plausibility of the concentration profiles

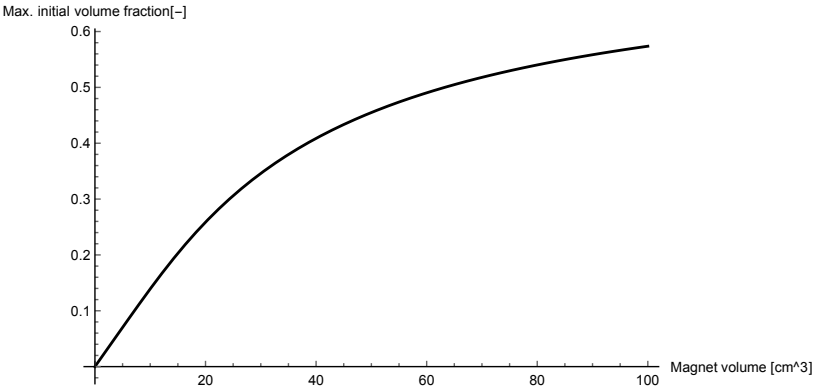


**Figure 3:** Maximum initial volume fraction against volume of a rectangular block magnet. The dimension of the magnet are $1 \times 1 \times 1$, the length of the ferrofluid column is 2 $cm$, the magnetic dipole moment corresponds to that of 10 nm particles and the temperature is room temperature $298K$.

for ideal magnetic dipoles, and one would expect significant corrections of the concentration profiles before the maximum volume fraction was violated. The reason the maximum volume fraction was violated is because the magnetic dipoles were assumed to be ideal point particles with no excluded volume in the thermodynamic theory. In the next section the concentration profiles for particles with excluded volume will be derived.

## 3.2 Dipoles with excluded volume in external fields

It seems that the approximation of the nanoparticles as ideal point particles gives non-physical results for realistic experimental conditions. This indicates that interactions should be taken into account. In this section two approaches will be taken. In the first approach the excluded volume interaction will be approximated by the second virial coefficient. As the second virial coefficient is not sufficient at high concentration ranges, the second approach will use the Carnahan-Starling equation of state [16] to account for the excluded volume interactions. It will be shown for the second virial description that the concentration profile has no analytical expression. Thus a general numerical method

for the calculation of concentration profiles for interacting particles will be presented.

**Second virial description:** The formalism with which non-ideal concentration profiles are described is the same as for ideal concentration profiles, but now with a different internal chemical potential. Chemical potential at all positions should be constant. Rewriting Eq.13 for an arbitrary function for the chemical potentials gives:

$$\mu_{int}(c(x)) - \mu_{int}(c(0)) = -\int_x^0 F_m(x')dx' \tag{25}$$

The mathematically simplest non-ideal case is taking the second virial coefficient into account, as this is a linear correction. The internal chemical potential from the second virial coefficient is [16]:

$$\mu(c) = \mu_0 + k_B T(\ln(c) + B_2 c) \tag{26}$$

The requirement for constant chemical potential then reads:

$$k_B T \ln(\frac{c(x)}{c(0)}) + k_B T B_2(c(x) - c(0)) = -\int_x^0 F_m(x')dx' \tag{27}$$

This is a linear-exponential function, which is solved by the Lambert-W function[17].

$$c(x) = \frac{W(c_0 B_2 \cdot \exp(c_0 B_2) \cdot \frac{H_0 \cdot \sinh(\zeta H(x))}{H(x) \cdot \sinh(\zeta H_0)})}{B_2} \tag{28}$$

The form of this function depends explicitly on $c_0$ and is not a linear scaling of the concentration profile as in the ideal description. Because of this we can not do a general analysis based on the reduced concentration $c(x)/c_0$. An additional complication is that the integral of the Lambert-W function only has an analytical expression published for a few special cases in limited ranges[17]. Such an integral is needed for any analysis based on the initial starting concentration, as can be seen for instance in Eq.24. This problem will likely only get more complicated when higher order virial coefficients are introduced. Equations of

state are generally higher order polynomials. An example is the chemical potential derived from the Carnahan-Starling equation of state of hard spheres:

$$\mu_{cs} = k_B T \frac{8\eta - 9\eta^2 + 3\eta^3}{(1-\eta)^3} \tag{29}$$

where $\eta$ indicates the volume fraction, defined by $\phi c$ where $\phi$ is the volume of a single particle. As the description of concentration gradients accounting for the second virial coefficient already requires the use of a numerical method, it seems logical to develop a numerical analysis method that is applicable for arbitrary equations of state. This was the motivation for the development of a general numerical method for the calculation of concentration profiles. This method will be described in the next subsection.

## 3.3 General numerical method

### 3.3.1 Concentration gradient, general expression

Again we start with the requirement of constant chemical potential. But instead of comparing two points at an arbitrary distance, two positions an infinitesimal distance apart will be considered.

$$\mu(c) + \mu(x) = \mu(c + \delta c) + \mu(x + \delta x) \tag{30}$$

Using the fact that the spatial integral of force is energy ($\int F_m(x)dx \equiv E(x)$) this equation becomes:

$$\mu(c) + E(x) - E(0) = \mu(c + \delta c) + E(x + \delta x) - E(0) \tag{31}$$

As $\delta c$ represents an infinitesimal variation, the first order Taylor expansion around $c$ and $x$ is exact.

$$\mu(c + \delta c) = \mu(c) + \frac{d\mu(c)}{dc}\delta c \tag{32}$$

$$E(x + \delta x) = E(x) + F_m(x)\delta x \tag{33}$$

Substituting this into Eq.31 gives:

$$-F(x)\delta x = \frac{d\mu(c)}{dc}\delta c \tag{34}$$

The physical significance of this formula is that in equilibrium, the force on the particles should be balanced out by a chemical potential gradient. This chemical potential gradient is the result of a concentration gradient. The required concentration gradient is given by the field and particle properties and reads:

$$\frac{dc}{dx} = \frac{-F(x)}{d\mu(c)/dc} \tag{35}$$

The function defines a concentration gradient for every $(x, c)$ coordinate. The concentration gradient needed to balance out the force does not only depend on the position $x$ but also on the concentration $c$. This can be understood intuitively by considering a collection of particles at almost the densest packing fraction and a dilute collection. Increasing the particle concentration will take more force for the closely packed particles than for the dilute particles. For true hard spheres the force will even become infinite. Because of this property, the concentration profile depends on the reference concentration $c_0$, the concentration at the bottom of the sedimentation vessel. The reference concentration can be calculated by using conservation of particles.

### 3.3.2 Concentration gradient for several thermodynamic potentials

**Ideal:**

$$\frac{dc}{dx} = -F(x) \cdot \frac{c}{k_B T} \tag{36}$$

Note that this also follows from the derivative of the barometric concentration gradient $dc/dx = -F(x) \cdot \frac{c}{k_B T}$

**Second virial coefficient:**

When dealing with hard spheres, it is more natural to work in terms of volume fraction $\eta$ instead of concentration. This can be done by the

substitution $c = \eta/\phi$, with $\phi$ the volume of one particle given by $\pi d^3/6$ .

$$\frac{dc}{dx} = -F(x)/(\frac{k_B T}{c} + 2k_B T B_2) \tag{37}$$

**Hard sphere virial**[16]:

$$\frac{d\eta}{dx} = -F(x)/(\frac{k_B T}{\eta} + 8k_B T) \tag{38}$$

**Carnahan-Starling**[16]:

$$\frac{d\eta}{dx} = -F(x) \cdot \frac{1}{k_B T}(\eta + \frac{(1-\eta)^3}{8 - 18\eta + 9\eta^2} + \frac{(1-\eta)^4}{8\eta - 9\eta^2 + 3\eta^3}) \tag{39}$$

### 3.3.3 Numerical integration method

After calculating the chemical potential gradient we can find the concentration profile by numerical integration. The numerical integration was done by the fourth order Runge-Kutta method[18]. This method involves iteratively finding four differentials, after which a weighed average is taken. The general structure for the numerical integration is given by:

$$\begin{cases} c_{n+1} = c_n + \frac{h}{6}(k_1 + 2k_2 + 2k_3 + k_4) \\ x_{n+1} = x_n + h \end{cases} \tag{40}$$

The factor $h$ is the step size in the $x$ position, which can be adjusted manually in the program. The variables $k_n$ are given by:

$$\begin{cases} k_1 = f(c, x) \\ k_2 = f(c + hk_1/2, x + h/2) \\ k_3 = f(c + hk_2/2, x + h/2) \\ k_4 = f(c + hk_3, x + h) \end{cases} \tag{41}$$

The function $f(c, x)$ is given by $d\eta/dx$ and depends on the magnetic field, particle size and chosen chemical potential. The fourth order Runge-Kutta method is used for initial value problems. In these

problems a starting point is taken from which the numerical integration starts. By choosing an arbitrary starting concentration at $x = 0$, a concentration profile is found by numerically integrating the curve. Integrating this curve again gives the number of particles. This can be repeated iteratively with a simple search algorithm to find a concentration profile that differs from the initial number of particles by an arbitrarily small error value. This arbitrary error value is also chosen manually. The actual code is implemented in Python 2.7.11, and can be found in Appendix A with comments.

### 3.3.4 Notes on attractive interactions

In a later section, it will be shown that using the Carnahan-Starling equation of state and hard sphere virial coefficients results in physically realistic concentration profiles. This is because they model repulsive interactions that lower the maximum volume fraction. When using second virial coefficients that model *only* attractive interactions, the predicted concentration profiles are even less physically valid than the ideal concentration profiles. To model attractive interactions such as magnetic attractions or van der Waals forces between particles higher order hard sphere terms still need to be taken into account to yield physical predictions. For a correct description the equation of state that models both hard sphere interactions and attractive interactions, such as dipolar or van der Waals attractions, is needed. At the time of writing this thesis no such equations of state are known for ferrofluids. In lieu of an equation of state, a crude approximation can be used to model the effects of attractive interactions. This is done by Taylor expanding the hard sphere equation of state into its virial components and substituting the lower order terms, such as the second or third virial coefficient for known attractive interactions. This will cause the low volume fraction behavior to be correctly governed by attractive interactions, while the high volume fraction interactions are correctly described by a divergence of the chemical potential at high volume fractions. The chemical potential of the intermediate volume fractions will not be the result of any theory, but will be an average of attractive and hard sphere interactions. A set of virial coefficients (second

and third) that will be very useful to consider are that of dipolar hard spheres in an external magnetic field[19]. With this method the effect of weakened magnetic coupling by longer polymer chains can be investigated, as well as other qualitative trends.

## 3.4 Example calculations

To illustrate the numerical method, calculations for the presented thermodynamic potentials will be shown. As a model system we will again use the experimental system from Berret[6]. In the experiment of Berret the field was relatively weak and the sedimentation vessel was small enough to consider the magnetic field gradient to be constant $\approx$ 10T/m. For the calculation a magnetic field, length of the fluid column, particle size and initial concentration must be assumed. We will present calculations for the experimental parameters used in the initial experiment from Berret, followed by calculations on a longer fluid column and slightly higher initial concentration.
The concentration profile below is calculated by the previously discussed methods, with a step size of $10^{-6}$ m and error margin of $10^{-8}$ m. It closely resembles the published profile by Berret for monodisperse systems, with a concentration decrease of a factor two over 2 mm. If the calculation is repeated taking into account the hard sphere viral coefficient and the Carnahan-Starling equation of state, all curves overlap. This indicates that the concentration range in the experiment is indeed in the ideal regime. When the system is made more concentrated and larger, the ideal approach will give non-physical predictions. This can be seen in a graph calculated for a system with an initial concentration of 3 volume percent and a length of 5 cm.

In the experiment of Berret, the magnetic field could be considered to be linear because the sedimentation vessel was extremely small compared to the magnet. In applications this is not necessarily the case. In the experimental work of this thesis, sedimentation of magnetic nanoparticles close to a very small magnet will be considered. The magnetic field of this magnet is only locally strong, and non-linear. The prediction for real non-linear magnetic fields can be found in the results section.

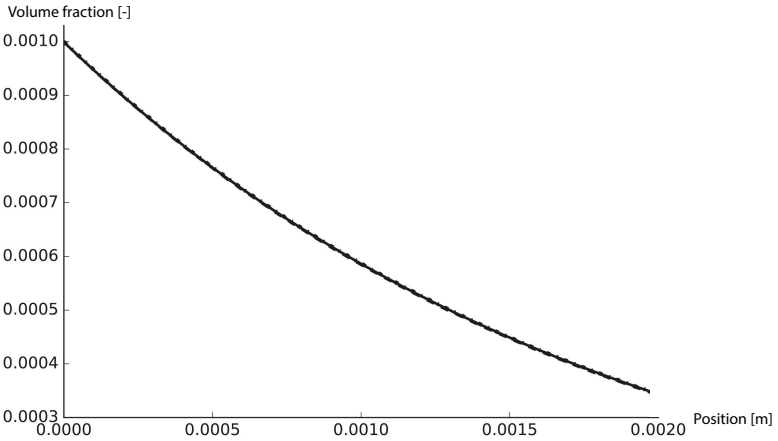


**Figure 4:** Plot of the volume fraction profile for the experiment of Berret, with 10 nm magnetite particles, system length of 2 mm, magnetic field gradient of 10 T/m. The concentration profiles are almost equal, indicating that the system can be approximated ideally.

# 4 Time-dependent description

## 4.1 Introduction and context

In Chapter 3 the equilibrium concentration profile of magnetic particles in strong fields was discussed. When or if this equilibrium profile is reached depends on how long a magnetic field is applied to the fluid. The timescale during applications can range from $10^4$ seconds or longer in magnetic pressure seals [4, 1], to several seconds in density gradient separation technology [3]. For pressure seals, maximum pressure as a function of time was measured. It was found that a seal would become stronger as function of time. This surprising finding is attributed to the sedimentation of particles in the applied magnetic field. The sedimentation of nanoparticles causes the magnetization near the magnet to increase, making the displacement of fluid energetically more unfavorable [4]. The pressure-time relation was calculated from the diffusion-drift equation[10]. This equation— also known as the Fokker-Planck

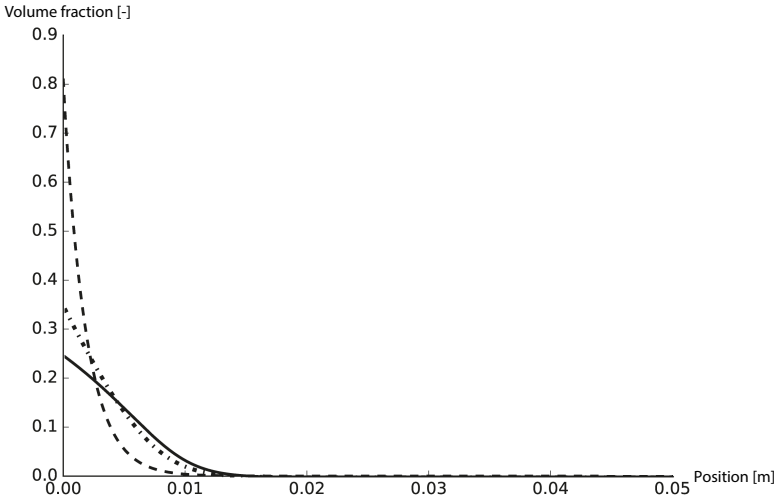


**Figure 5:** Plot of the predictions for a hypothetical, more concentrated and larger scale, version of Berret's experiment. Continuous line corresponds to the Carnahan-Starling equation of state prediction, point-dash corresponds to the second virial hard sphere prediction and the dashed line is the ideal prediction. Note that the ideal prediction is non-physical as it goes over the highest packing fraction of 0.74.

equation— describes concentration profiles as a function of time [1]:

$$\frac{\partial c}{\partial t} = \frac{\partial}{\partial x}\left(\frac{Dc(x)}{k_B T}\frac{d\mu(c(x))}{dx} - vc(x,t)\right) \tag{42}$$

For ideal particles this equation is manageable because of the simple expression for the chemical potential. Even in this case the equation is not always analytically solvable. Time dependent solutions, the so called Faxen's solutions, are known for the cases of no diffusion, no sedimentation or infinitely long tubes[20]. From these solutions, approximations can be made for the cases of little diffusion, little sedimentation

[1] This equation is often used as the basis for solving the equilibrium concentration profile by solving for $\frac{\partial c(x)}{\partial t} = 0$[6, 7, 13]

or long tubes [20]. The solutions when found are extremely information dense, describing the concentration at every time and position. For the pressure seals, an attempt was made to solve this equation in complex geometries[4]. The experimental system described was very complicated, involving magnetohydrodynamics, fluid rotations and complicated magnet geometry. The calculated value for the sedimentation timescale was two orders of magnitude faster than the real experimental value ($\tau_{calc} \approx= 10^{-2}t^{-1/2}$ versus $\tau_{exp} = 8.4 * 10^{-3}t^{-1/2}$). The difference was ascribed to the sensitivity of the calculations to the experimental values used[4].

As the previous section examined the importance of (excluded volume) interactions, it makes sense to take these into account while solving the diffusion-drift equation. If this is not done, the end state where there is no concentration change will converge on a wrong concentration profile. Adding these non-ideal terms introduces non-linear terms to the differential equation, which makes solving the resulting equation much more difficult than it originally was. The effect of particle interactions on the hydrodynamic friction factor is described by Batchelor[21]. Here the excluded volume interactions manifest themselves into the backflow of fluid and the distribution of the stress field through the liquid. However, this only affects the hydrodynamic friction factor. As such this correction will not make the diffusion-drift equation converge on the correct equilibrium profile.

As there is no accessible theoretical description of the timescale found for easily realized test systems, a new model will be proposed in the next section. The aim of this model is to find a time scale for the sedimentation, not to describe the concentration at all positions and times. The idea behind this model is to deal with the non-ideal interactions by comparing the non-ideal equilibrium profile with the starting concentration profile, instead of implementing it in a differential equation. The final equation has a form that is often found for overdampened relaxation processes. Thus the model can be interpreted as the relaxation of an initial state to a known equilibrium. Considering that the equilibrium concentration profile had to be calculated

numerically with the tools given by thermodynamics, it is not surprising that calculating this profile starting from the diffusion equation is difficult. The diffusion equation is needed to find a time scale, as thermodynamics contains no kinetic information and only gives information about equilibria.

### 4.1.1 Fundamental assumption

The fundamental assumption for this model is that the concentration changes monotonically. By making this assumption, the point shared by the starting and equilibrium concentration profiles (the intersection where $c(x, t = 0) = c(x, t = \infty)$) becomes a stationary point, as will be discussed in the next section. The diffusion through this stationary point is given by Fick's first law. Fick's first law is less complicated than the diffusion-drift equation, as it is not a differential equation. The assumption for monotonic concentration changes is valid if a point where the concentration increases never has a decreasing concentration, and vice versa. This is observed in many sedimentation experiments and an example will be given in the results section of this thesis. The mathematical expression for this assumption is that:

$$\mathrm{sgn}(\frac{d}{dt}c(t)) = \text{constant} \tag{43}$$

In other words, this assumption means that the sign of $dc/dt$ is *locally* constant at all times. Another interpretation is that the concentration change can never be *away* from the local equilibrium.

## 4.2 Model

As a first step, it will be derived that the intersection between the starting and equilibrium concentration profiles is indeed a stationary point. The condition for the intersection is that the concentration on the stationary point $s$ at $t = 0$ is equal to the concentration at $\lim_{t\to\infty}$. This can be rewritten as

$$\int_0^\infty \frac{d}{dt}c(s,t)dt = 0 \tag{44}$$

The only expression for $\frac{d}{dt}c(s,t)$ that satisfies Eq.43 is:

$$\frac{d}{dt}c(s,t) = 0 \tag{45}$$

As such, the point $x = s$ is a stationary point where the concentration does not change. Everywhere else in the sedimentation vessel the concentration does change. As there is conservation of particles, the only way in which this concentration change can be facilitated is by flowing through the stationary point. For the one-dimensional sedimentation experiment this reads:

$$\int_0^\infty dt \int_0^s dx \frac{\partial}{\partial t}c(x,t) = \int_0^\infty J(s,t)dt \tag{46}$$

As the average concentration change over the entire sedimentation vessel is 0, the relation between the concentration change in the region $s \geq x \geq 0$ and $L \geq x \geq s$ can be derived.

$$\int_0^L dx \frac{\partial}{\partial t}c(x,t) = \int_0^s dx \frac{\partial}{\partial t}c(x,t) + \int_s^L dx \frac{\partial}{\partial t}c(x,t) = 0 \tag{47}$$

The concentration change in each of these regions is dictated by the flow through the stationary point. This shows that by knowing the flux of particles through the stationary point, the average concentration changes in regions above and below the stationary point are known. This gives less information than solving the diffusion-drift equation, as not the full concentration as function of position and time is known, but this approach will still result in a useful time scale.

$$\int_0^s dx \frac{\partial}{\partial t}c(x,t) = -\int_s^L dx \frac{\partial}{\partial t}c(x,t) = J(s,t) \tag{48}$$

In the next section the flow through the stationary point will be found.

### 4.2.1 Flow through stationary point

The flux of particles through a point is given by the average speed of a particle times the concentration of particles.

$$J(x,t) = v(x,t) \cdot c(x,t) \tag{49}$$

Evaluated in the stationary point, where concentration is constant through time, this becomes:

$$J(s,t) = v(s,t) \cdot c(s) \tag{50}$$

where $v$ indicates the speed of an average particle. Now the time dependency of the sedimentation is given only by the speed of particles in the stationary point. This speed can then be further decomposed in an time independent body force and a time dependent term. The strength of the force $F$ is determined by the strength of the external magnetic, gravitational and centrifugal fields at the stationary point $s$. There is also an effective thermodynamic force, given by the chemical potential gradient $\frac{d\mu}{dx}$, whose strength is determined by the concentration gradient at the stationary point $s$, which in turn depends on time. The frictional coefficient $w$ is considered to be constant, in line with the constant concentration $c$. The resulting expression for the speed is:

$$wv(s,t) = F(s) + \frac{d\mu(c(s,t))}{dx} = F(s) + \frac{d\mu(c(s))}{dc} \cdot \frac{dc(s,t)}{dx} \tag{51}$$

### 4.2.2 Approximating the concentration gradient in the stationary point

The chemical potential term is problematic, as it depends on the concentration gradient. The concentration gradient in turn depends on the exact concentration profile $c(x,t)$. In the introduction we showed that finding the concentration profile as function of time was problematic.

For the special case where the stationary point is either close to

the top or the bottom of the vessel this problem can be circumvented. When this condition is met, the concentration profile in the smallest section can be approximated by the first order Taylor expansion in $c(x = s)$. Thus the derivation shown is exact only for the case where the stationary point is infinitely close to a border of the sedimentation vessel. The result that will be derived this way can also be found by assuming the concentration gradient scales linear with the total integrated flux $\int_0^t J(s,t')dt'$. Here $t'$ is a dummy integration variable.

Taking $s \ll L$, the function $c(x,t)$ equals its first order Taylor expansion in the region $0 \leq x \leq s$.

$$c(x,t) = c(s) + b(t)(x-s) \text{ where } b(t) = \frac{dc(s,t)}{dx} \tag{52}$$

Now the trick is to find $b$ as function of time. Using Eq. 48 and 50 we find:

$$w \int_0^t dt' \int_0^s dx \frac{\partial}{\partial t'} c(x,t') = \int_0^s c(x,t) - c(s) dx = \int_0^t J(s,t')dt' \tag{53}$$

This equation simply states that any increase of the concentration in the region between 0 and $s$ is due to the flux through the stationary point. As between the boundary of the second integral the Taylor expansion Eq.52 is valid, this can be substituted for $c(x,t)$.

$$\int_0^t J(s,t')dt' = \int_0^s b(t)(x-s)dx = -\frac{b(t)s^2}{2} \tag{54}$$

Substituting this result into Eq. 50 gives an expression for $J(s,t)$ in the form of an ordinary differential equation. If one assumes a linear relation between the concentration gradient and the total integrated flux they immediately arrive at this equation using a self consistency from equilibrium argument.

$$\frac{w}{c(s)} J(s,t) = F(s) - \frac{d\mu(c)}{dc} \cdot \frac{2}{s^2} \int_0^t J(s,t')dt' \tag{55}$$

This equation can be solved to find an expression for $J(s,t)$, which

describes the speed of the entire sedimentation process. However, it carries some cumbersome terms that are not directly experimentally measurable and intuitively not quite clear. Using the fact that in the limit of $t \to \infty$ there is no flux, and defining $\int_0^\infty J(s,t)dt \equiv \Delta n$, Eq.55 gives:

$$\frac{F(s)}{\Delta n} = \frac{d\mu(c)}{dc} \cdot \frac{2}{s^2} \tag{56}$$

As $\Delta n$ can be easily directly measured in sedimentation experiments and found from calculated equilibrium concentration profiles, through the relations in Eq.54, this will be used to rewrite Eq.55. Taking the derivative of this equation with respect to time gives the clearest view of the ordinary differential equation that must be solved.

$$\frac{dJ(s,t)}{dt} = -\frac{F(s) \cdot c(s)}{w\Delta n} J(s,t) \tag{57}$$

A first order differential equation requires a single boundary condition. At $t = 0$ there is no concentration gradient, so a suitable boundary condition is that at $t = 0$ the flux through the stationary point must be:

$$J(s,0) = \frac{F(s) \cdot c(s)}{w} \equiv J_0 \tag{58}$$

Solving the differential equation and substituting the newly defined $J_0$ an extremely simple expression for the speed of sedimentation is found. All variables can be calculated just by knowing the starting conditions, equilibrium profile and the field strength.

$$J(s,t) = J_0 \exp(-\frac{J_0}{\Delta n} \cdot t) \tag{59}$$

Two striking characteristics of this expression are the intuitive expression for the characteristic time $\tau = J_0/\Delta n$ (the initial flux divided by the total concentration change) and the self consistency with the previously defined $\Delta n$. This equation has a form that is often seen for over dampened relaxation phenomena, which is a novel interpretation of a sedimentation process.

We can compare the timescale from this theoretic description to that of another commonly used method. This other timescale calculates the time it takes for a single particle to sediment from the top of the vessel to to the bottom. These two timescales are not equal. This can be seen when considering the small magnet limit, where a particle at the top of the sedimentation vessel will feel no field. This will cause the sedimentation time for a particle to go to infinity, while the presented method will result in a finite time scale, indicating that the presented method is more suitable for magnetic sedimentation.

# 5 Experimental: measurements and synthesis

The measurement of concentration profiles of magnetized ferrofluids is interesting both out of fundamental interest and applications. For applications the stability of a ferrofluid in a magnetic field is directly related to concentration profiles. In the search for more stable ferrofluids, the quantitative and even qualitative characterization of stability is difficult because of the opaque black nature of ferrofluids, complicating the use of conventional optical measurement methods. This makes the screening and testing stages of ferrofluid development labor intensive. Equilibrium concentration profiles can also be used to explore fundamental physics. A concentration profile gives information on thermodynamic properties resulting from the particle interactions, such as magnetic interactions or the previously explored hard sphere interactions[22, 23, 24]. As for the simple dipolar hard sphere and Stockmayer fluids no full equation of state is known, experimental clues on how these systems behave are desirable.
The previously presented theoretical extension for the incorporation of hard sphere repulsions showed that correcting for hard sphere interactions often results in qualitatively different predictions, both in timescale and equilibrium state. However, hard sphere interactions are but one possible correction in a variety of complications present in real ferrofluids. A noteworthy example is polydispersity, for which it has been shown that it can significantly alter equilibrium concentration profiles[6]. Other effects that can dominate sedimentation in ferrofluids are for instance magnetic coupling and its effect on viscosity[25]. These complicating effects are not accounted for in the present theory. Experiments are necessary to evaluate the importance of these effects. It is shown theoretically that the hard sphere correction is significant, but only experiments can show if the hard sphere description is useful.

In this section of the thesis a detailed description of the setup and implementation of the analytical centrifugation experiments will be given. Special attention will be given to the measurement of particle properties and the magnetic field so a comparison between the theory

and experiments can be made with no fit parameters. The measurement method makes use of an analytical centrifuge, which speeds up measurements and gives an extra control parameter.

## 5.1 Analytical centrifugation

The Stability Analyzer LUMiFuge® was used for analytical centrifugation. It was originally designed to study the sedimentation kinetics of industrial dispersions or foodstuffs by changes in light transmission. The advantages of the LUMiFuge® over the traditionally used analytical ultracentrifuges is the relatively low rotation rate which allows for the use of heavy particles and the larger wavelength used, which colloids often absorb less. Standard plastic sample holders with an optical path length of 2 mm are used, but in this sample holder a custom built capillary with an optical path length of 0.3 mm is placed in which the ferrofluid is held.
The transmission is measured as a function of radial position, which in turn is measured as function of time. A pulsed NIR-LED illuminates the sample cell at a wavelength of 880 nm and the transmitted light is detected by a CCD-line of 2048 elements positioned every 14 $\mu$m[22]. Previous work identified that optical broadening gives a final resolution of 400$\mu$m. The rotation rate ranges from 200 to 4000 rpm. Twelve sample cells can be placed on the rotor and be measured in unison.

### 5.1.1 Capillary construction

A $50 \times 3 \times 0.3$ mm$^3$ capillary was glued onto a microscope slide. It is important only to glue the edges of the capillary to the slide, in order to prevent optical distortions in the middle of the capillary where the ferrofluid will be. A zirconium oxide spacer was glued to the glass walls of a capillary by instrument makers using a brush made of a single metal wire. Care was taken that no glue went into the capillary, which was confirmed for every capillary by visual inspection. The spacers were cut to custom sizes and measured with a caliper. Zirconium oxide, which is opaque, was preferred over glass as it is was found that reflections in the glass illuminated the ferrofluid from below during transmission measurements. The capillaries were filled with ferrofluid by a gel tipped

Finnpipette. The top of the capillary was molten and closed with a clamp. The following step was done was done as quickly as possible as to minimize the unmeasured sedimentation. A magnet was positioned under the spacer with a drop of UV-glue and hardened under an ultraviolet lamp. The capillaries were added to centrifuge tube and the measurement was started. The time from magnet placement to measurement was approximately ten minutes for twelve samples.

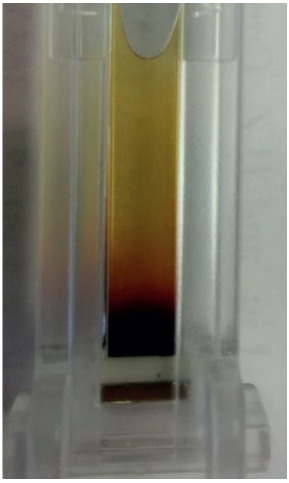

**Figure 6:** Picture of a capillary filled with ferrofluid, picture taken after centrifugation measurement.

### 5.1.2 Data analysis

Raw text files were extracted from the LUMiFuge program SepView 6.0 by pressing shift and clicking on the measurement in the measurement tab. The data was converted to a Mathematica data file with a prewritten script (LUMReader.m), which was also used in [22]. The minimum transmission of the entire measurement ($T_{min}$) is subtracted from the signal before analysis, as the LUMiSizer records a finite transmission even for opaque materials like magnets. Previous work has shown that this is a digital artifact [22]. The transmission data was converted to

absorption using the formula:

$$A(x) = -^{10}\log(\frac{T(x)}{T_0(x)}) \tag{60}$$

The transmission $T$ and absorption $A$ are denoted as function of position to highlight the fact that the normalization is done separate for every spatial measurement point by taking the local transmission at time zero, $T_0$. There is a background of light loss from reflections and absorption of solvent and glass. This background is accounted for by subtracting the average absorption of a region with no colloids present measured at the end of the sedimentation, given by:

$$A_b = -^{10}\log\frac{T^*_{end}}{T^*_0} \tag{61}$$

Here $T^*_{end}$ and $T^*_0$ are averages calculated by integrating over a range virtually free of colloids and dividing by the integration length. The absorption by colloids is then given by $(1/l\int_0^l T(x)dx)$:

$$A_{col}(x) = A(x) - A_b = -^{10}\log(\frac{T(x)}{T_0(x)}\frac{T^*_0}{T^*_{end}}) \tag{62}$$

The absorption can be converted to concentration by assuming that Lambert-Beer is valid, which gives a linear relation between concentration and absorption, and by assuming the initial concentration profile is homogeneous and has a known concentration $c_i$.

$$c(x,t) = \frac{A_{col}(x,t)}{A_{col}(x,0)}c_i \tag{63}$$

It is often seen in measurements that the transmission spectra in the first half minute have unexpected features. This is attributed to the movement of fluid and air in the capillary. Because of this, usually the measurement obtained after a minute of centrifugation is used for normalization. A check for optical saturation, the regime where Lambert-Beer is no longer valid, is that the integrated absorption should be constant at all times. This was coded into the Mathematica script, and the measurement was accepted as valid if there was no more than 5% difference between the integrated absorption of initial and end pro-

files.

Time dependent data analysis was done by inspecting the region of decreasing absorption by eye and checking if the stationary point was indeed stationary. The concentration in this region was then integrated and divided by the length to give the average concentration as function of time.

## 5.2 Ferrofluid synthesis

For the comparison between theory and experiments it is important to have a model system in which effects that are not accounted for in the model are as small as possible. The two most influential effects are polydispersity and particle clustering. While charged particles are potentially very interesting, the study of charge is outside the scope of this work. Approximately charge neutral particles can be realized by using organic apolar solvents with a low dielectric constant. Particle clustering in these solvents is usually prevented by a surfactant layer adsorbed on the particles. This polymer layer prevents two particles being so close that they have strong (attractive) interactions. However, magnetic particles with magnetic domains larger than 10 nm can show chain forming behaviour when aligned in magnetic fields[26]. These chains form because the externally applied magnetic field aligns the particles, strengthening the attractive magnetic interactions by aligning particles in the head to tail configuration[26]. While this effect can be surpressed by using extremely long polymer chains, this would introduce further complications such as a large hydrodynamic radius and a potential soft sphere interaction. Because the sedimentation of chains is an entirely different problem, the chain forming behaviour limits the maximum particle size that can be used.
In this section the synthesis of two different model systems, corresponding to magnetite and maghemite particles, will be described.

### 5.2.1 Hyeon synthesis

What we will call the Hyeon synthesis is the synthesis of magnetite nanoparticles based on thermal decomposition of iron salts[27]. Be-

cause of the high temperature needed to decompose the salts, a solvent with a high boiling point has to be used during the synthesis. The boiling point of the solvent determines the reaction temperature, as the reaction is done during reflux. The reaction temperature influences the particle size, and because of this the solvent choice influences particle size. It is important to note that the precise solvent-size relation from the original Hyeon paper could was not reproduced, but the result differed a few nanometer in diameter. Strengths of the Hyeon synthesis method are the low polydispersity in comparison with other single step synthesis methods and the relative degree of size control. Weaknesses are the difficulty associated with the synthesis of magnetic nanoparticles smaller than 10 nanometer and the fact that large nanoparticles can have multiple magnetic domains[28].

**Iron salt precursor synthesis**

The iron-oleate precursor complex was prepared by addition of 20 mL ethanol, 15 mL millipore water, 35 mL octadecene, 9.1 g sodium oleate and 2.7 g $Fe(III)Cl_3 \cdot 6H_2O$ to a roundbottom flask. A water condenser was fixed on the roundbottom flask, which in turn was connected to the nitrogen source. The mixture was heated to 70°C in an oil bath for approximately 4 hours under a nitrogen atmosphere. The system separated into a brown organic top layer and an aquaous bottom layer. The top layer was retrieved by using a separating funnel and washed three times with 15 mL demiwater. The washing and separating steps should be done gently as to prevent the oil and water layers forming an emulsion. After washing volatile contaminants, such as ethanol and water, were removed in the rotavap under vacuum at 50°C, yielding the iron oleate product dissolved in octadecene as a dark brown oil. The precursor synthesis can also be done in hexane as apolar solvent instead of octadecene. When done so, after the vacuum extraction the final product will be pure iron oleate, allowing spectral analysis and yield calculation.

**Particle synthesis**

It is known that the thermal decomposition of the iron oleate complex is sensitivily dependent on the heating rate. For this reason a heating

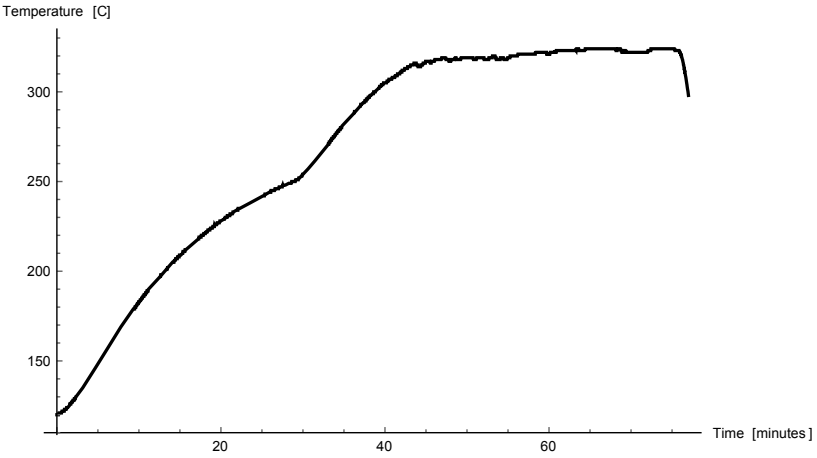


**Figure 7:** Temperature as function of time for the Hyeon particle synthesis.

mantle with an adjustable power supply was used to control the heating rate. In the heating mantle sits a roundbottom flask connected to a water condenser with a mechanical stirrer. The water condenser was connected to both a nitrogen source and vacuum pump, allowing the application of a nitrogen atmosphere immediately after degassing without allowing oxygen to enter. The synthesis is sensitive to atmosphere leaks in the tubing. The heating response as measure of the power voltage was measured with 50 mL octadecene until it started refluxing. This information was used to try and achieve a heating rate of 4°C per minute. The solvent was cooled down and replaced with 30 mL octadecene, 20 mL of the precursor solution and 230.5 mg oleic acid. The power supply was set to 93 volt and a vacuum was applied. The solution was degassed for two and a half hours at 120°C. After two and a half hours the vacuum pump was shut off and a nitrogen atmosphere was applied. The power supply was set to 170 volt and after a half hour the solution was 250 °C. The power supply was set to 210 volt and after fifteen minutes the solution was 310 °C. After another 15 minutes, the solution was allowed to cool down. Total reaction time was 1 hour and 15 minutes.

**Workup**

100 mL ethanol and 300 mL cyclohexane were added to cooled reaction product and centrifuged at 3500 rpm. The fluid was decanted off while holding a magnet under the phase separated mixture to keep the nanoparticles in place (magnetic decantation). The solid was washed three times with a 50 mL ethanol/cyclohexane mixture (1:1) and then allowed to dry in the fumehood (with cover against dust). The solid was succesfully redispersed in 30 mL decalin. The workup of the Hyeon particles is tedious as it is difficult to destabilize the magnetite particles. The destabilization is done by addition of an anti solvent for the oleic acid surfactant, which should initiate clustering of the particles. It is found however that much larger amounts of anti solvent are needed than previously reported in the literature, making workup labor intensive as large volumes of suspension have to be centrifuged. This is why the particles are not redispersed after every washing step, but instead the destabilized particles are kept in an anti solvent during the washing steps. The particles were analyzed by TEM and VSM.

### 5.2.2 Massart synthesis

The Massart synthesis is a classical synthesis of maghemite particles by the coprecipitation of iron(II) and iron(III) salts[29]. The synthesis is very easy and robust, but the resulting particles are very polydisperse. To reduce the polydispersity, a size fractionation step was done after the particle synthesis[30]. The size fractionation works by destabilizing the charge stabilized particles by the addition of salt. The salt screens the particle charges and allows the particles to cluster. As larger particles have stronger attractions this allows for the somewhat selective sedimentation of particles. After the size fractionation the particles are coated with oleic acid and redispersed in decalin.

**Particle synthesis**

8.68 gram of $FeCl_3 \cdot 6H_2O$ and 3.29 gram of $FeCl_2 \cdot 4H_2O$ were dissolved in 380 mL demiwater. During vigorous stirring 25mL 28% ammonia was added. The solution was stirred for 5 minutes and was magnetically decanted. The particles were redispersed in 40 mL 2M $HNO_3$. 8.48 gram $FeNO_3 \cdot 9H_2O$ was added and the solution was heated to

90°C. After an hour the solution was removed from heat and the particles were magnetically decanted. The particles were washed twice with 2M nitric acid and redispersed in 210 mL demiwater.

**Size fractionation**

10.2 mL 65% nitric acid was dissolved in 75 mL demiwater to form a stock solution used for the size fractionation. After the addition of 40 mL of this stock solution to 210 mL of the product from the previously described synthesis the solution became somewhat turbid. A magnet was placed under the solution and after several minutes, the fluid was magnetically decanted into two volumes with a ratio of roughly 2 : 1 (top-bottom). The bottom fraction (bot) was redispersed by diluting to a final volume of 150 mL. 5 mL of the acid stock solution was added to the top fraction and a large amount of dark brown precipitate formed. After magnetic sedimentation for several minutes, the solution was magnetically decanted in 2 : 1 ratio again. The bottom fraction (top-bot) from this separation was redispersed by diluting to 100 mL. To this fraction (top-bot) 10 mL of the acid stock was added, and the precipate was magnetically decanted in a 2 : 1 ratio. From the bottom fraction (top-bot-bot) all fluid was decanted as to keep only the sediment. To the bottom layer of the first decantation (bot) 20 mL of the acid stock solution was added. The precipitate was magnetically sedimented and magnetically decanted in a 2 : 1 ratio. Previous experiments had shown that the bottom-bottom fraction consists of mostly aggregates and thus it was discarded. To the top fraction (bot-top) 10 mL of the acid stock solution was added and again magnetically sedimented and decanted in a 2 : 1 ratio. The bottom fraction was diluted to a final volume of 50 mL and redispersed. The fractions were given the following names. Top-top=S1, top-bottom-top=S2, top-bottom-bottom=S3, bottom-top-top=S4, bottom-top-bottom=S5.

**Particle coating and work up**

A couple of hours passed between the fractionation and work up, and in this time a tiny sediment layer had formed. Because of this, all solutions were magnetically decanted again to remove the solid. The top-top layer was diluted to a final volume of 200 mL and a 30% am-

monia solution was added drop wise. After the addition of 3 mL 30% ammonia all particles had sedimented and the remaining solution was colourless. The precipitate was magnetically decanted and only the solid was kept. The precipitate was washed twice with 100 mL water. 100 mL water was added and everything was added to a separatory funnel. 10 mL of liquid oleic acid was added and the system was vigorously shaken. Afterwards the organic layer was deep brown and a significant fraction stuck to the glass of the separatory funnel. The aqueous layer, white and turbid, was separated. The organic layer was washed twice with 100 mL water, and the last fraction was colourless and clear. The organic phase was washed out of the separatory funnel with approximately 20 mL ethanol. The solid was magnetically sedimented and washed thrice with 20 mL ethanol. The wet slurry was covered and dried overnight under a nitrogen stream. This procedure, with variable addition of ammonia, was repeated for all fractions. The following morning the slurries had dried and cracked, and changed color from brown to black. The solids were weighed and redispersed in approximately 10 mL decalin and weighed again. The top-bot-bot fraction would not redisperse so 5 drops of oleic acid were added. After this the solid would redisperse.

## 5.3 Particle analysis

Particle size distributions were measured by vibrational sample magnetometer (VSM) and transmission electron microscopy (TEM). The size characterization by separate methods is necessary as one would expect different values for the magnetic and hard sphere radii. The methods approximately measure these radii. It is known that most particle size distributions of nanoparticles in ferrofluids are well described by log normal functions instead of normal Gaussian functions [31]. In the low polydispersity limit these two functions are approximately equal [6]. The description of the particle size distribution is particularly important because it is found that concentration profiles change significantly from the ideal exponential function as the polydispersity is increased. The description of this effect uses the log normal standard deviation. To ensure that any deviations of a barometric concentration profile are due to the excluded volume and not due to polydispersity the log

normal standard deviation has to be lower than 0.2. For ease of interpretation and some of the later analysis we also report the normal standard deviation, even though the fit is generally somewhat worse.

| **VSM measurements** | | |
|---|---|---|
| Sample | Weight [mg] | Sat. magnetization [$10^{-5}$A/m] |
| H1 | 54.6 | 5.168 |
| S1 | 57.3 | 25.55 |
| S2 | 42.4 | 9.05 |
| S3 | 54.3 | 30.70 |
| S4 | 40.8 | 8.50 |

**Table 1:** VSM sample weights and saturation magnetization. No paramagnetic correction was performed. The measurements were done in plastic cups of approximately 200$\mu$L.

**VSM** Samples were weighed in VSM sample holders and suspended in the magnetic field. Magnetization loops were measured and average particle sizes were calculated with the MINORIM software package[32]. The average particle size is found by a linear fit around $M(H = 0)$, from which the average particle size can be recovered via the linearization of the Langevin function around $H = 0$.

From the saturation magnetization the volume fraction of magnetic material can be calculated.

$$\eta_{mag} = \frac{M_{sat}}{M_{vol}}/V = \frac{M_{sat}m}{M_{vol}\rho} \tag{64}$$

where $M_{vol}$ is the volume magnetization, $4 \cdot 10^5$ and $4.8 \cdot 10^5$ A/m for maghemite and magnetite respectively, $M_{sat}$ is the measured saturation magnetization, $V$ is the sample volume. The sample volume is calculated by dividing the sample weight by the density of the solvent, which for decalin is 896 kg/m$^3$. Note that the magnetic volume fraction is not equal to the volume fraction used in the thermodynamic theory, as it does not take account any non magnetic material on the particle. The magnetic volume fraction can be converted to a hard sphere volume fraction using the following formula:

$$\eta_{part} = \eta_{mag} \frac{(r_{tem} + \delta)^3}{r_{vsm}^3} \tag{65}$$

Here $\delta$ stands for the length of the surfactant in nm, which for oleic acid is $\approx 1.5$ nm. In the literature there are often reports of a magnetically inactive surface on the particles. Whether such a dead surface layer is present can be checked by TEM measurements and will show up as a discrepancy between the magnetic and TEM radii. The contribution of this dead surface layer to the volume fraction is accounted for by the use of $r_{tem}$ in the numerator.

**TEM** For the TEM analysis the ferrofluids were diluted approximately by a factor hundred in cyclohexane. A drop of the suspension was pipetted on the Formvar coated copper TEM grid and the grid was dried under a heat lamp for approximately an hour. The images were analyzed with the iTEM software package. The three point circle measurement tool was used by choosing three points on the edge of the particle in such a way that the center of the particle coincided with the centre of the circle. The Mathematica NormalLogFit function was used on the resulting size distribution. The use of the three point circle measurement method is not standard. The standard method is the measurement of the diameter as the distance between the most distant borders of the particle in a predetermined axis. This method was deemed unsuitable because the measurement of one single particle for 100 different choices of the predetermined axis gave a polydispersity of 5 nm for this one particle. This particle had the volume corresponding to a sphere with a 10 nm diameter. This indicates that orientation averaging of the rough irregular particles with this measurement method creates artificial polydispersity in the magnetic moments of the particles that does not represent reality.

## 5.4 Experimental characterization of magnetic fields

**Analytical function of the magnetic field**

The magnetic field is a vector quantity, whose local value does not only have a magnitude but also a direction. This vector can be de-

constructed in Cartesian coordinates in scalar magnetic fields corresponding to the $x$, $y$ and $z$ dimensions. An analytical expression for these magnetic fields is reported in [33]. We will denote the axis going perpendicular to the magnetic pole the $x$ axis, and the axis parallel to the long direction of the magnet the $y$ axis. We are only interested in the sedimentation towards the magnet so only the $x$ component of the magnetic field vector will be considered. It was found that found that the magnetic field was approximately translationally invariant of the $y$ and $z$ coordinates along the magnet length, allowing us to describe the magnetic field by an one dimensional scalar function $H_x$.

$$H_x(x) = \frac{M_r}{\pi}(\arctan\frac{LW}{(2x\sqrt{4x^2+L^2+W^2})} - \arctan\frac{LW}{2(R+x)\sqrt{4(R+x)^2+L^2+W^2}}) \tag{66}$$

Here $L$ is the length of the magnet, $W$ is the width of the magnet, $R$ is the thickness of the magnet and $M_r$ is the remanent magnetization of the magnet. The units of the remanent magnetization determine the units of the magnetic field. The magnetic field gradient is given and defined by the derivative $\frac{dH_x}{dx}$, and for our rectangular block magnet it reads:

$$\frac{dH_x}{dx} = \frac{2M_rLW}{\pi}(-\frac{L^2+W^2+8x^2}{(L^2+4x^2)(W^2+4x^2)\sqrt{L^2+W^2+4x^2}} + \frac{L^2+8R^2+W^2+16Rx+8x^2}{(4R^2+W^2+8Rx+4x^2)(L^2+4(R+x)^2)\sqrt{L^2+W^2+4(R+x)^2}}) \tag{67}$$

**Magnetic field measurements**

The magnetic field of the magnets used was measured using a magnetic Hall probe, encased in a protective aluminum cover. The magnetic Hall probe was fixed on an cathetometer using an aluminum clamp. The cathetometer was zeroed at first contact between the Hall probe and the magnet, where after the magnet was moved laterally underneath the probe until the position with the maximum magnetic field was found. The Hall probe was slowly removed from the magnet

while the distance and magnetic field were recorded. The measurement was repeated with the Hall probe upside down. If the effective measurement point in the Hall probe was exactly centered in the casing the same magnetic field would be measured. The thickness of magnetic probe was measured with a calliper and was found to be 1.65 mm. The two measurements were fitted onto each other with a distance offset as fit parameter. The fit quality was inspected by eye and an optimal fit was found for an offset of 0.7 mm. From this the effective measurement point in the probe could be calculated and the magnetic field strength could be plotted as the function of the absolute distance. The analytical function of the magnetic field of a rectangular bar magnet of $5 \times 1.5 \times 1\text{mm}^3$ with a remanent magnetization of 1.3 T (the advertised magnetization) and the measurement do not match. With a remanent magnetization of 1.05 T an excellent fit between experiments and theory was obtained.

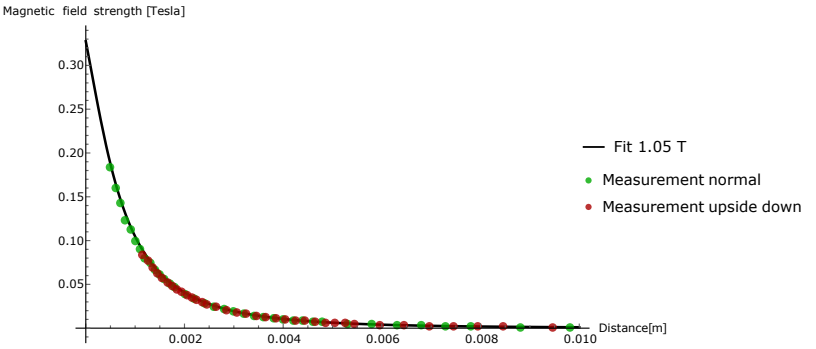


**Figure 8:** The fit between the measurement and analytic function for a rectangular bar magnet. The results of the two measurement orientations were fit on each other by an offset. From this offset the measurement point was determined. The measurement does not go to zero because of the finite thickness of the magnetic Hall probe (Lakeshore Gaussmeter 455).

**Concentration-dependent magnetic permeability** Magnetic field propagation depends on the magnetic permeability of the material. The magnetic permeability depends on the magnetizability of the material, which for ferrofluids depends linearily on the concentra-

tion of particles (if independent magnetic moments are assumed). In equilibrium the concentration profile is given by the magnetic field. The concentration profile and magnetic field should be self-consistent in equilibrium. The relation between the concentration profile and the magnetic field is determined by the non-linear Langevin function, as this determines the magnetizability. Because of this an analytical solution for this problem does not seem tractable and finite element analysis was used. Finite element analysis has the additional benefit of accounting for the potentially significant contribution of edge effects.

A neodymium magnet with dimensions of $5 \times 1.5 \times 1$ mm$^3$ and remanent magnetization of 1.05 T was constructed in the commercial finite element software package, MagNet Infolytica 7.7.1. On this magnet 20 compartments of $1 \times 0.3 \times 0.1$ mm$^3$ were constructed, placed 0.1 mm from the magnets edge. This represents the thickness of the glass capillary wall. A range of custom materials was defined representing the magnetization of different concentrations of ferrofluids, as per the Langevin function.

$$M(\phi) = \phi M_{sat} L(\zeta H) \tag{68}$$

With this method, the assumption of independent magnetic moments of the Langevin function is used. First the concentration profile with no magnetic permeability correction was calculated with the Carnahan-Starling equation of state as described in the theory. This was done for the capillary construction as described with no spacer. These concentration profiles were coarse grained in 0.1 mm and 0.3 volume percent intervals and these were entered in the finite element software using the boxes and custom materials previously described. With starting concentrations under the ten volume percent, no significant change in the final magnetic field was found. At higher starting concentrations the magnetic field became weaker and it could be reasonable approximated by the magnetic field of the same magnet with a lower remanent magnetization. This magnetic field was used to calculate a new concentration profile and this process was repeated until the result did not change significantly (3 iterations), ensuring that the concentration profile and the magnetic field influenced by its magnetic

permeability are self consistent.

The first relevant conclusion for the experimental work and interpretation ought to be that the effect of the permeability correction became discernible at $\eta_i \approx 0.1$. As this is an order of magnitude higher than the experimental conditions, it is safe to neglect the effect of the permeability correction for our experiments. While the effect at low volume fractions can be neglected, this previously undescribed effect becomes significant in our experimental geometry by lowering the effective remanent magnetization of the magnet by more than 0.1 T. In our simulated system the permeability correction has features that are characteristic for counter ion condensation in electrostatic systems. In our system compression of particles with a magnetic dipole by a strong magnetic field gradient source shields the source in such a way that the final field is approximately described by the field of an effectively weaker source. In electrical condensation compression of electrical monopoles by a strong electric field shields the source in such a way that the electric field can be approximately described by a rescaled weaker source. As there is only one experimental system simulated and there is no theoretical indication that these two effects are in any way analogues this similarity should be interpreted as an experimental observation. The conclusion relevant for this work is that the magnetic permeability correction can be safely neglected as even without a spacer the effect only becomes discernible at $\eta_i \approx 0.1$.

# 6 Experimental results and theoretical interpretation

## 6.1 TEM size distribution

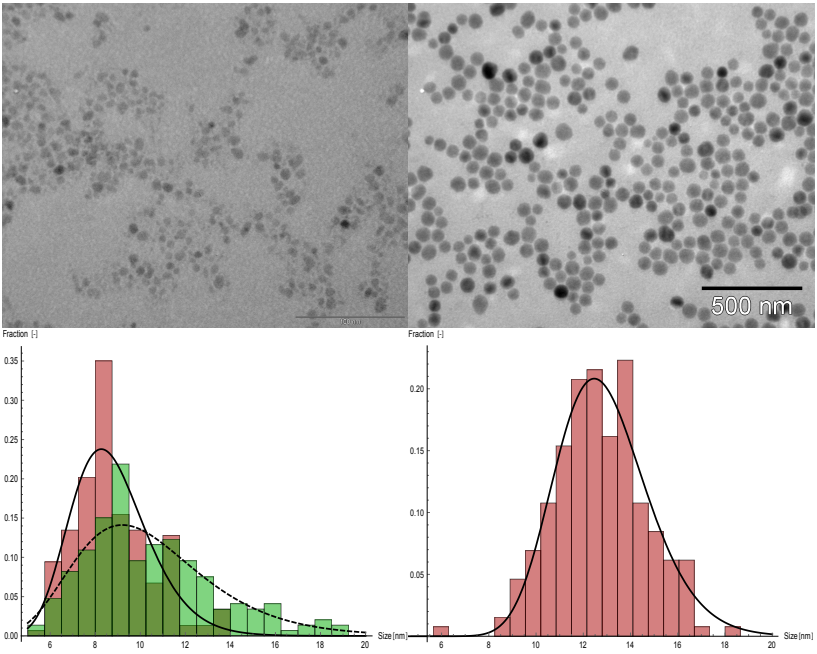


**Figure 9:** TEM images and size distributions of the magnetic nanoparticles. Left top: TEM image of the top-top fraction S1 from the Massart synthesis. Right top:TEM image of the particles from the Hyeon synthesis. Left bottom: Size distributions of the top-top fraction (red) S1 and the original Massart ferrofluid(green). The black lines are the best log normal fits to their respective distribution (continuous=fractioned, dashed=unfractioned). S1 average=8.8 nm, S1 std.=1.3 nm. Motherfluid average=10.5 nm, motherfluid std.=3.2nm. Right bottom: Size distribution of the Hyeon ferrofluid with the best log-normal fit. Average=12.9nm, std.=1.9nm.

There are two clear trends that can be seen in the particle size distribution from the fractionation series. The average particle diameter and polydispersity decrease when going down from the top fractions to

the bottom fractions. Comparing the TEM size distributions (Fig.9) of the S1 (top-top) fraction and unfractioned mother fluid reveals that fractionation mostly removes the largest particles. This results in the removal of the long tail of the log normal distribution, simultaneously lowering the polydispersity and the average particle diameter. Further analysis of the bottom fractions shows that the removal of small particles from the bottom fraction is much less efficient. This leads to a slightly higher polydispersity for the bottom fractions over the top fractions. The third fractionation step does not seem to decrease the polydispersity significantly over the two-step fractionation reported in the literature[30]. The log-normal and normal fit of the Hyeon particle size distribution are approximately equal. The polydispersity for both fits is small (1.9 nm). The fit can be seen in Fig.9.

## 6.2 VSM size distributions

The particle and magnetic diameters for the Massart particles are almost equal for an assumed volume magnetization of $4 \cdot 10^5 \mathrm{A/m}$. While it is often reported in the literature that magnetic particles have a poorly crystallized surface layer that is magnetically inactive, this layer does not seem to be present for the Massart particles. For the Hyeon particles, the magnetic diameter is much lower than the TEM diameter. The reported magnetic diameter was calculated with a volume magnetization of $4.84 \cdot 10^5 \mathrm{A/m}$. In the literature it is sometimes reported that the volume magnetization of nanoparticles is lower than for bulk material, but even with a volume magnetization of $4 \cdot 10^5 \mathrm{A/m}^2$ the magnetic diameter is significantly lower than the particle diameter. For the hard sphere theory it is not the magnetic diameter that is important but rather the magnetic moment of a particle, which is measured directly in the VSM. Because of this the question of the actual bulk magnetization could be disregarded, if it was not for the possibility of multiple magnetic domains. For roughly spherical particles it is not possible to fit two magnetic domains with a diameter of 9 nm into a particle with a radius of 13 nm. Therefore it will be assumed there is only one magnetic domain present in each particle. This indicates that the particles are poorly crystallized and have a large inactive surface layer [26].

| | S1 | S2 | S3 | S4 | S5 | Hy. |
|---|---|---|---|---|---|---|
| **VSM diam.** | 8.8 | 9.2 | 10.1 | 10 | - | 8.9 |
| **TEM diam.** | 8.8 | 9.3 | 9.3 | 10.2 | 10.9 | 12.9 |
| **VSM std.** | 1.3 | 1.5 | 2.1 | 2.0 | - | 1.0 |
| **TEM std.** | 1.7 | 2.2 | 2.1 | 2.5 | 2.1 | 1.9 |
| **TEM log std.** | 0.20 | - | 0.22 | - | 0.23 | 0.15 |
| **Magnetic vol.** | 0.010 | 0.005 | 0.013 | 0.005 | - | 0.016 |
| **Particle vol.** | 0.024 | 0.011 | 0.023 | 0.011 | - | 0.089 |

**Table 2:** Values for the TEM (particle) and VSM (magnetic) diameters in [nm] and the volume fraction occupied by magnetic material and particles. A surfactant size of 1.5 nm was used for the conversion from magnetic to particle volume fraction. Hy. stands for the Hyeon ferrofluid.

## 6.3 LUMiSizer results

It has to be noted that a significant fraction of measurements show unreliable results. A variety of different factors caused uncertainties in the measurements, and the most common issues will be highlighted here. The measurements in which these issues occurred will be disregarded, and thus only a small subset of measurements we believe to be reliable will be analysed thoroughly.

### 6.3.1 Common practical problems

**Optical saturation** The majority of measurements had to be discarded because the integrated absorption of the initially homogeneous state is not (approximately) equal to the integrated absorption of the final state. This was attributed to optical saturation, and a variety of sources were identified. The first source is the starting concentration. Using a starting concentration that is either so low that all light passes through or so high that no light passes through causes discrepancies with later concentration profiles. This can be understood by considering that a significant portion of sedimentation will be unobserved until the concentration is within the valid measurement range. The

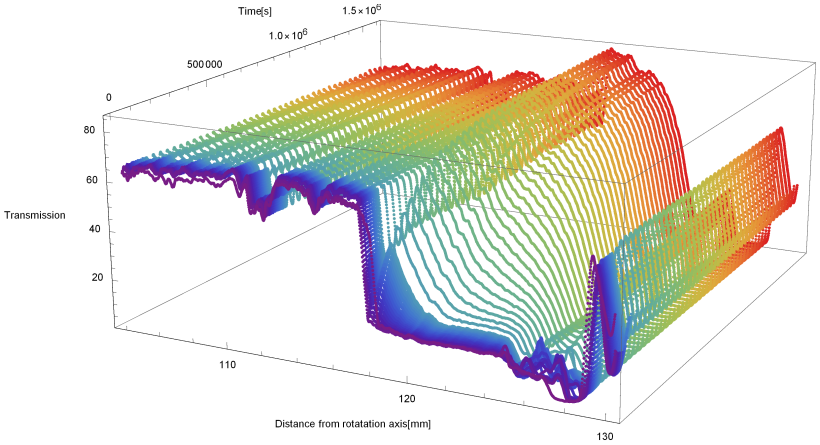


**Figure 10:** Plot of the raw transmission data as gathered from the LUMiSizer. Note the significant difference between the first profile and the second. Measurement has significant optical saturation present, as will be discussed in the time dependent results section. The time between these two measurements is 1 second, indicating this change is due to fluid movement.

second source is the optical saturation that occurs within the region of increasing concentration. This problem can be circumvented by only analysing the concentration profile in the spatial range where the concentration is within the concentration measurement range. However, there is no rigorous way to check where this range is. The third source is attributed to optical broadening close to the spacer or magnet. As both the spacer and magnet do not allow light to transmit, optical broadening of the fluid-solid edge can obscure a region of high concentration ferrofluid. This effect is hard to differentiate from the second source. Optical broadening is different from optical saturation in that the loss of integrated absorption does not occur at a certain threshold concentration. Instead, absorption is lost near the opaque bottom of the sample and the maximum concentration for the same sample differs between samples.

**Fluid movement** It is often seen in the beginning of a measurement that changes in the transmission occur that cannot be understood

through sedimentation. A common example is a change in the length of the fluid column in the capillary, or movement of the fluid column. This is attributed to fluid movement during the initial application of the centrifugal field. Such movement can occur over a time scale of minutes. If a long time is chosen between measurements (e.g. hours) then no reliable concentration profile corresponding to a homogeneous initial state could be used. If the time scale for the fluid movement to die out is long enough for significant sedimentation to occur then the same is true. This was checked by seeing if the final concentration profiles changed significantly if either of two successive measurements near the start of the experiment were chosen for the initial concentration profile. If this was the case the measurement was discarded.

**Evaporation and leakage** The decrease of overall volume over long time scales was attributed to either leaking, or evaporation in earlier capillary designs. With leaking an unknown amount of particles is lost, and thus the measurement cannot be interpreted reliably. With the final capillary design, less than 8% of capillaries showed leaking or evaporation (0 out of 12). In earlier capillary designs, all (open) capillaries showed significant evaporation and $\approx 10\%$ of capillaries glued directly to a magnet or glass spacer showed signs of leaking. This was concluded by optical inspection where particles were found on the magnet.

### 6.3.2 Equilibrium analysis

The first analysis will be done for the S1-top fraction of the Massart system. The ferrofluid was diluted (S1:decalin=1:1), giving a final concentration of 1.2 volume percent. The sample was centrifuged at 500 rpm for 24 days. Unfortunately, the sample did not reach equilibrium in this time. This was followed by centrifugation at 2000 rpm for another 24 days, in which the sample did reach equilibrium. This was concluded from the fact that the concentration did not change for several days. The measurement was done in duplo and the equilibrium profiles can be seen in Fig.11, together with the predictions from the Carnahan-Starling equation of state for particles with a diameter of 7.5, 8.8 and 10.1 nm for the described conditions. These values corre-

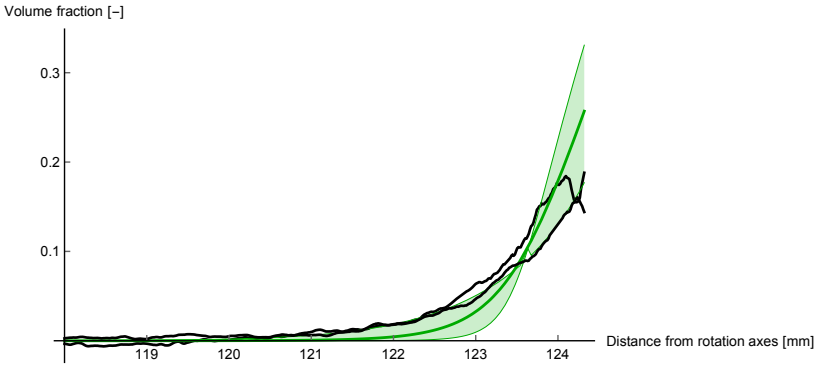


**Figure 11:** Equilibrium concentration profiles of the diluted S1 ferrofluid (S1:decalin=1:1) at 2000 rpm on a $5 \times 1.5 \times 1$ mm magnet at 1.03 mm separation. Black lines correspond to two separate measurements. Green lines correspond to predictions calculated with the Carnahan-Starling equation of state. The middle green line corresponds to the prediction for the average particle size of 8.8 nm. The upper and lower green line correspond to predictions for particles one standard deviation (1.3 nm) removed from this average size. The fluid column runs from 107 to 124.3 mm. The top centimeter of the fluid column is not depicted for readability.

spond to the the average and one standard deviation up or down from the average. Both measurements have $\approx 1\%$ loss of initial integrated absorption, from which it is concluded that optical saturation is negligible. For the numerical integration and search an error margin of $10^{-8}$ m and step size, correspond to $h$ in the theory, of $10^{-5}$ m was chosen. The length of the ferrofluid column was measured to be 1.7 cm.

It can be seen that the predictions agree with each other within a 20 percent margin of error (calculated from the reference concentration at the bottom from the vessel). A multitude of sources could be responsible for this error, both theoretical and experimental. For instance sample polydispersity, dipolar coupling, and optical line broadening, or a combination of these effects can reasonably be expected to cause corrections on this order of magnitude. A 20 percent error is significant, even for a zero fit prediction, but the real test is how the hard sphere prediction fares against the ideal prediction. This comparison

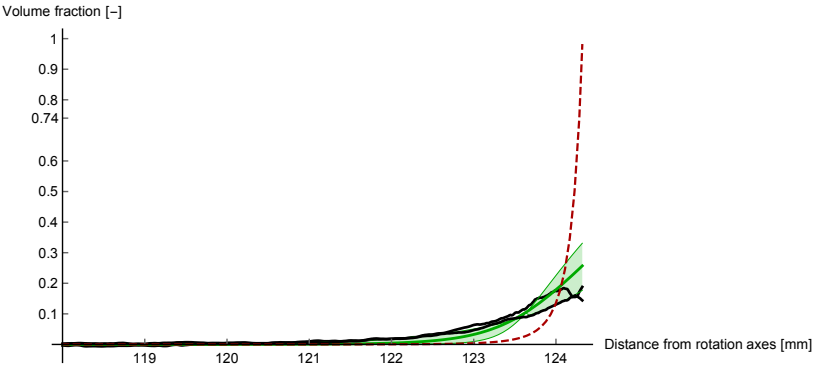


**Figure 12:** Hard sphere predictions (green) and ideal predictions (dashed red) compared to measurements (black). The ideal prediction has a maximum concentration larger than the densest sphere packing, at $\approx 102$ volume percent.

is made in Fig.12. It can be seen that the ideal prediction is unphysical and has a 500 percent margin of error. From this we conclude that the hard sphere description is needed to understand the measured concentration profiles.

It must be noted that in this measurement the centrifugal energy plays a larger role than the magnetic energy. The centrifugal energy of a particle can be calculated by using:

$$E_{cent} = \int_{x0}^{x.end} u\omega^2 x dx \tag{69}$$

where $x_0$ is the location of the meniscus, $x_{end}$ is location of the bottom of the sedimentation vessel, $u$ is the buoyant mass of a particle and $\omega$ is the rate of rotation in $[rad/s]$. The magnetic energy of a particle is approximately given by $\mu_0 m H_{max}$. Using $x_0 = 107$ mm, $x_{end} = 124.3$mm and $H_{max} = 8 \cdot 10^5$ A/m we find $E_{cent} \approx 10^{-19}$ [J] and $E_{mag} \approx 10^{-20}$[J]. The thermal energy of a particle is $E_{therm} = k_B T \approx 10^{-21}$[J]. This indicates that the centrifugal energy dominates in this measurement, as it is 10 times larger than the magnetic energy. However, the magnetic energy still has a significant contribution, and

is an order of magnitude larger than the thermal energy. Calculations, hard sphere and ideal, without magnetic field differ significantly from the presented predictions.

### 6.3.3 Time-dependent analysis

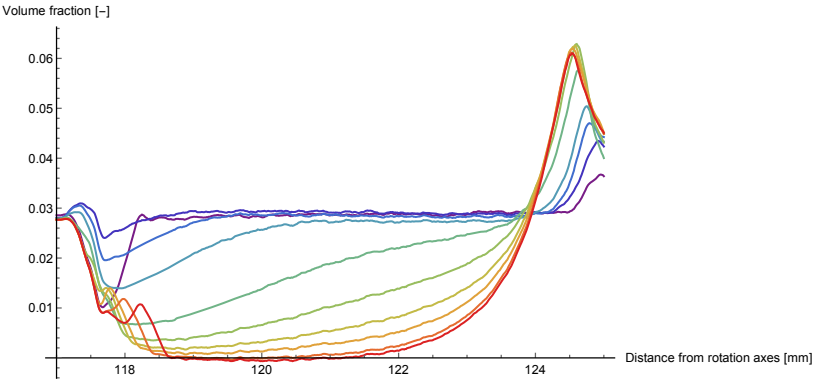


**Figure 13:** Concentration profiles at different times. All the profiles are roughly three days apart. The colder colours correspond to earlier times. It can be seen that optical absorption is present in the region between 124 and 125 mm after 12 days of sedimentation, as the absorption in this region does not increase after this time.

In Fig.13 the concentration profiles at several different times for the Hyeon system measurement can be seen. The spacer distance was 1.84 mm, and the sample was centrifuged at 500 rpm. The Hyeon ferrofluid was diluted by a factor three, to a final concentration of 3 volume percent. There is significant optical saturation, which can be clearly seen by eye in Fig.13. Between the first and the last measurement, $\approx$ 70 percent of integrated absorption is lost. While this invalidates the analysis of the entire concentration profile, the time dependent analysis can be performed on this sample. $J_0$ was calculated by using the centrifugal and magnetic fields to calculate the force on a particle at the stationary point. The friction was calculated using the Stokes friction, where the TEM radius was used for the particle size. For the spacer length of 1.84 mm the strength of the magnetic field is insignificant, but it is still taken into account. The value for the viscosity of

decalin used was 1.6 mPa · s [34].

As a first observation it can be seen in Fig.13 that the fundamental time dependent assumption, that at every point the concentration changes monotonically, holds. The stationary point that results from this observation is located at 123.8 mm from the rotation axis. Determining the location of the meniscus is not easy, as a approximately half a millimeter of decalin evaporates during the experiment. This also introduces error during the analysis, which is difficult to characterize exactly. It is chosen to locate the meniscus at 117.9 mm. With these values characteristic time and initial flux for the average concentration between the meniscus and stationary point can be calculated. This was done both for the ideal thermodynamic potential and Carnahan-Starling potential. The magnet was identified at 124.5 mm. The results can be seen in Fig.14.

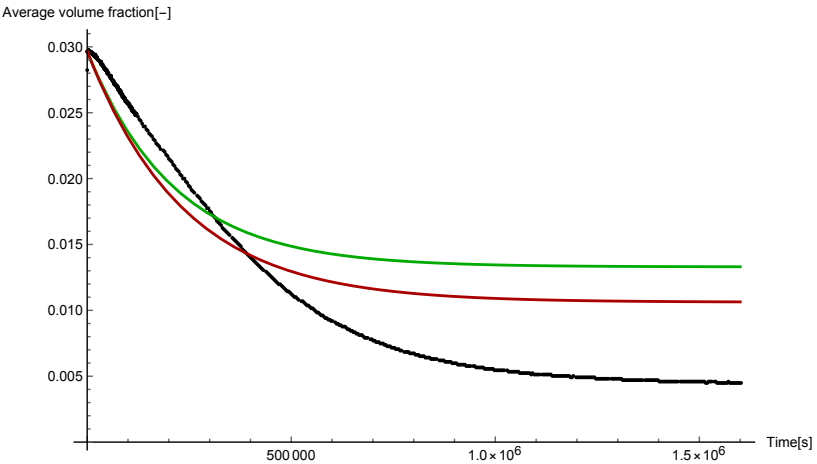


**Figure 14:** Measured average concentration (black) in the region from 117.9 mm to 123.8 mm as function of time compared to the predictions from hard sphere (green) and ideal (red) theory.

While both methods approximate the time scale of sedimentation reasonably, there are several problems. The hard sphere prediction are almost equal, but the ideal prediction seems to perform slightly bet-

ter than the hard sphere prediction. Both experiments underestimate the total amount of particles sedimenting. This and the finding that the hard sphere prediction is worse can potentially explained by the weak magnetic and centrifugal field. This could cause the maximum concentration of particles to be in the regime where attractions dominate. The effect of attractions has shown to have significant effects on the concentration profiles of magnetic nanoparticles in the intermediate concentration range [22, 23]. Another possibility for the bad fit is that the condition where the concentration profile can locally be approximated by a Taylor expansion is not valid.

# 7 Conclusion

An analytical function for the equilibrium concentration profile of magnetic dipoles was derived. It was found that for our experimental set-up the ideal description predicted concentration higher than the highest packing fraction. A numerical method for concentration profiles of non ideal particles was derived. It was shown that for the second virial description the concentration profile can be described by the Lambert-W function. Equilibrium concentration profiles were measured in the LUMiSizer analytical centrifuge. To our knowledge this is the first direct measurement of concentration profiles in macroscopic non-linear magnetic fields and in a centrifuge. Ferrofluids were synthesized to obtain well defined model systems and this allowed for a zero-fit comparison of the ideal and hard sphere theories. It was found that the ideal theory was unphysical and the hard sphere theory using the Carnahan-Starling equation of state fit the data well. As both the non-ideal particles and arbitrary magnetic fields are difficult to describe by the diffusion-drift equation, new theory was developed to extract a time scale of sedimentation. The timescale from this theory matches the experimental timescale, however the final average concentration does not match the experiments.

# 8 Acknowledgements

I would like to thank Ben Erné for supervision, feedback and being a great teacher of the scientific method and scientific research. I would like to thank Alex van Silfhout for his practical advice and experimental collaboration. Henk-Jan Siekman is thanked for the fabrication and design of the capillary in which the measurements were done. Albert Phillipse, Dominique Thies-Weesie, Bonny Kuipers, Joeri Opdam and Stijn Bruning are thanked for helpful discussion and support.

# 9 Appendix A: Numerical integration code

Code written for Python 2.7—Anaconda 4.0, uses numpy and matplotlib. Run in Spyder

In this section the experimental details of the system are entered. All units are in SI units. A rectangular bar magnet is assumed. The error parameter is the arbitrary error as discussed in the thesis. The amount of steps determines the coarseness of the numerical integration.

```
import numpy as np
import matplotlib .pyplot as plt

a = 0.73 * 10** - 8#Particle diameter[m]
mu = 1.256 * 10** - 6#Magnetic permeability
B = 1.05 * 795774#Magnetic field strength at magnet[A/m]
k = 1.38064852 * 10** - 23#Boltzmann constante[J/K]
T = 298#Temperatuur[K]
magnetization = 4 * 10**5#Volumetric magnetization[Am^2]
zeta = (mu * np.pi * magnetization * (a)**3/(6 * k * T))
labda = zeta * k * T
omega = 2000/60 * 2 * np.pi  #centrifugation speed[Radian/s]
m = (4300 * np.pi * a**3)/6#delta mass of one particle[kg]
L = 0.005#length of magnet[m]
W = 0.0015#Width of magnet[m]
R = 0.001#Thickness of magnet[m]
error = 0.000000001
steps = 300#Amount of steps for numerical integration of one line

#Used for centrifugal field
mm_from_rotation_axis = 106.5 * 10** - 3
```

These two options are only used when an equation of state influenced by magnetic coupling is used.

```
polymer_length = 0.1 * 10** - 8#[m]
coupling = (mu * (np.pi/6 * magnetization * a**3)**2)/(4 * np.pi * k * T * (a + polymer_length)**3)
```

The magnetic field for a rectangular bar magnet and its spatial derivative. The first option is the linear magnetic field assumed in the Berret experiment. These functions have to be manually copied into the dir function, which is the implementation of Eq.35.

```
#Magnetic field strength Berret : B − 10 ∗ 800000 ∗ h
#Magnetic field strength : (B/np.pi) ∗ (np. arctan((L ∗ W)/(2 ∗ h ∗ (4 ∗ h**2 + L**2 + W**2)**0.5))
−np. arctan((L ∗ W)/(2 ∗ (R + h) ∗ (4 ∗ (R + h)**2 + L**2 + W**2)**0.5)))
#Derivative magnetic fieldstrength : (((2 ∗ B ∗ L ∗ W)/np.pi)∗
(−(((L**2 + W**2 + 8h**2)/((L**2 + 4 ∗ h**2) ∗ (W**2 + 4 ∗ h**2) ∗ (L**2 + W**2 + 4h**2)**0.5))+

((L**2 + 8R**2 + W**2 + 16R ∗ h + 8h**2)/((4R**2 + W**2 + 8R ∗ h + 4h**2)
∗(L**2 + 4(R + h)**2) ∗ (L**2 + W**2 + 4(R + h)**2)**0.5)))))
```

Here the derivatives for the ideal, second virial hard sphere and Carnahan-Starling hard sphere chemical potentials are implemented together with the magnetic field and magnetic field derivative functions for rectangular bar magnets. The functions are normally commented out and have to be manually copied into the working dir function to work. The addition of $10^{-}100$ is to circumvent division by zero errors.

```
Carnahan-Starling equation of state and magnetic field rectangular block magnet : dir =
−1/(k ∗ T ∗ ((1/phi) + ((8 − 18 ∗ phi + 9 ∗ phi**2)/(1 − phi)**3) + ((24 ∗ phi − 27 ∗ phi**2 + 9 ∗ phi**3)
/(1 − phi)**4))/(((h + mm_from_rotation_axis) ∗ m ∗ omega**2)+
((1/np. tanh((zeta ∗ ((B/np.pi) ∗ (np. arctan((L ∗ W)/(2 ∗ (h + 10** − 100)∗
(4 ∗ (h + 10** − 100)**2 + L**2 + W**2)**0.5)) − np. arctan((L ∗ W)/(2 ∗ (R + (h + 10** − 100))∗
(4 ∗ (R + (h + 10** − 100))**2 + L**2 + W**2)**0.5)))))) − (1/(zeta ∗ ((B/np.pi)
∗(np. arctan((L ∗ W)/(2 ∗ (h + 10** − 100) ∗ (4 ∗ h**2 + L**2 + W**2)**0.5))−
np. arctan((L ∗ W)/(2 ∗ (R + (h + 10** − 100)) ∗ (4 ∗ (R + (h + 10** − 100))**2 + L**2 + W**2)**0.5)
))))) ∗ (labda ∗ ((((2 ∗ B ∗ L ∗ W)/np.pi) ∗ ((((L**2 + W**2 + 8 ∗ (h + 10** − 100)**2)/
((L**2 + 4 ∗ (h + 10** − 100)**2) ∗ (W**2 + 4 ∗ (h + 10** − 100)**2) ∗ (L**2
+W**2 + 4 ∗ (h + 10** − 100)**2)**0.5)) + ((L**2 + 8 ∗ R**2 + W**2
+16 ∗ R ∗ (h + 10** − 100) + 8 ∗ (h + 10** − 100)**2)/((4 ∗ R**2 + W**2 + 8 ∗ R ∗ (h + 10** − 100)+
4 ∗ (h + 10** − 100)**2) ∗ (L**2 + 4 ∗ (R + (h + 10** − 100))**2)**0.5)))))))))

Ideal chemical potential and magnetic field rectangular block magnet : dir =
−1/(k ∗ T ∗ ((1/phi)) /(((h + mm_from_rotation_axis) ∗ m ∗ omega**2)+
((1/np. tanh((zeta ∗ ((B/np.pi) ∗ (np. arctan((L ∗ W)/(2 ∗ (h + 10** − 100)∗
(4 ∗ (h + 10** − 100)**2 + L**2 + W**2)**0.5)) − np. arctan((L ∗ W)/(2 ∗ (R + (h + 10** − 100))∗
(4 ∗ (R + (h + 10** − 100))**2 + L**2 + W**2)**0.5)))))) − (1/(zeta ∗ ((B/np.pi)
∗(np. arctan((L ∗ W)/(2 ∗ (h + 10** − 100) ∗ (4 ∗ h**2 + L**2 + W**2)**0.5))−
np. arctan((L ∗ W)/(2 ∗ (R + (h + 10** − 100)) ∗ (4 ∗ (R + (h + 10** − 100))**2 + L**2 + W**2)**0.5)
))))) ∗ (labda ∗ ((((2 ∗ B ∗ L ∗ W)/np.pi) ∗ ((((L**2 + W**2 + 8 ∗ (h + 10** − 100)**2)/
((L**2 + 4 ∗ (h + 10** − 100)**2) ∗ (W**2 + 4 ∗ (h + 10** − 100)**2) ∗ (L**2
+W**2 + 4 ∗ (h + 10** − 100)**2)**0.5)) + ((L**2 + 8 ∗ R**2 + W**2
+16 ∗ R ∗ (h + 10** − 100) + 8 ∗ (h + 10** − 100)**2)/((4 ∗ R**2 + W**2 + 8 ∗ R ∗ (h + 10** − 100)+
4 ∗ (h + 10** − 100)**2) ∗ (L**2 + 4 ∗ (R + (h + 10** − 100))**2)**0.5)))))))))
```

```
Chemical potential second virial hard sphere and magnetic field rectangular block magnet  : dir =
−1/(k ∗ T ∗ ((1/phi) + second_virial)
/(((h + mm_from_rotation_axis) ∗ m ∗ omega**2)+
((1/np.tanh((zeta ∗ ((B/np.pi) ∗ (np.arctan((L ∗ W)/(2 ∗ (h + 10** − 100)∗
(4 ∗ (h + 10** − 100)**2 + L**2 + W**2)**0.5)) − np.arctan((L ∗ W)/(2 ∗ (R + (h + 10** − 100))∗
(4 ∗ (R + (h + 10** − 100))**2 + L**2 + W**2)**0.5)))))) − (1/(zeta ∗ ((B/np.pi)
∗(np.arctan((L ∗ W)/(2 ∗ (h + 10** − 100) ∗ (4 ∗ h**2 + L**2 + W**2)**0.5))−
np.arctan((L ∗ W)/(2 ∗ (R + (h + 10** − 100)) ∗ (4 ∗ (R + (h + 10** − 100))**2 + L**2 + W**2)**0.5)
))))) ∗ (labda ∗ ((((2 ∗ B ∗ L ∗ W)/np.pi) ∗  ((((L**2 + W**2 + 8 ∗ (h + 10** − 100)**2)/
((L**2 + 4 ∗ (h + 10** − 100)**2) ∗ (W**2 + 4 ∗ (h + 10** − 100)**2) ∗ (L**2
+W**2 + 4 ∗ (h + 10** − 100)**2)**0.5)) + ((L**2 + 8 ∗ R**2 + W**2
+16 ∗ R ∗ (h + 10** − 100) + 8 ∗ (h + 10** − 100)**2)/((4 ∗ R**2 + W**2 + 8 ∗ R ∗ (h + 10** − 100)+
4 ∗ (h + 10** − 100)**2) ∗ (L**2 + 4 ∗ (R + (h + 10** − 100))**2)∗
(L**2 + W**2 + 4 ∗ (R + (h + 10** − 100))**2)**0.5))))))))
```

Function calculates the derivative as per Eq.35. The explicit function containing the chemical potential derivative, magnetic field and Langevin function has to be entered manually. Examples for rectangular bar magnets can be found above. The arguments of the function distance ($h$), magnetization of the magnetic field source ($B$), the magnetic moment of the particle times the magnetic permeability ($labda$) and volume fraction ($phi$). The output of the function is the double dir, which represents the local derivative. The first line has the option to add an offset (in meters), which can be used to represent a spacer.

```
def direction(phi, h, B, labda) :
h = h + 1 ∗ 10** − 3#Determines spacer distance
if(phi ∗ labda ∗ B ∗ 3 == 0) : #this makes sure that there is no overflowerror when the concentration goes to0
dir = 0
else : #Expansie Carnhan − Starling met field − dependent dipolar hardsphere correctie
dir =
Carnahan-Starling equation of state and magnetic field rectangular block magnet  : dir =
−1/(k ∗ T ∗ ((1/phi) + ((8 − 18 ∗ phi + 9 ∗ phi**2)/(1 − phi)**3) + ((24 ∗ phi − 27 ∗ phi**2 + 9 ∗ phi**3)
/(1 − phi)**4))/(((h + mm_from_rotation_axis) ∗ m ∗ omega**2)+
((1/np.tanh((zeta ∗ ((B/np.pi) ∗ (np.arctan((L ∗ W)/(2 ∗ (h + 10** − 100)∗
(4 ∗ (h + 10** − 100)**2 + L**2 + W**2)**0.5)) − np.arctan((L ∗ W)/(2 ∗ (R + (h + 10** − 100))∗
(4 ∗ (R + (h + 10** − 100))**2 + L**2 + W**2)**0.5)))))) − (1/(zeta ∗ ((B/np.pi)
∗(np.arctan((L ∗ W)/(2 ∗ (h + 10** − 100) ∗ (4 ∗ h**2 + L**2 + W**2)**0.5))−
np.arctan((L ∗ W)/(2 ∗ (R + (h + 10** − 100)) ∗ (4 ∗ (R + (h + 10** − 100))**2 + L**2 + W**2)**0.5)
))))) ∗ (labda ∗ ((((2 ∗ B ∗ L ∗ W)/np.pi) ∗  ((((L**2 + W**2 + 8 ∗ (h + 10** − 100)**2)/
((L**2 + 4 ∗ (h + 10** − 100)**2) ∗ (W**2 + 4 ∗ (h + 10** − 100)**2) ∗ (L**2
+W**2 + 4 ∗ (h + 10** − 100)**2)**0.5)) + ((L**2 + 8 ∗ R**2 + W**2
+16 ∗ R ∗ (h + 10** − 100) + 8 ∗ (h + 10** − 100)**2)/((4 ∗ R**2 + W**2 + 8 ∗ R ∗ (h + 10** − 100)+
4 ∗ (h + 10** − 100)**2) ∗ (L**2 + 4 ∗ (R + (h + 10** − 100))**2)∗
```

```
(L**2 + W**2 + 4 * (R + (h + 10** - 100))**2)**0.5)))))))))
return dir
```

In this function the derivative calculating function *dir* is numerically integrated to yield a concentration profile. The calculation method is fourth order Range-Kutta. The arguments of this function are a starting concentration $phi_0$, a starting location $h_0$, an end point $h_{end}$ and a step size $dh$, usually given by $h_{end}/steps$. The output of this function is a list of locations (h_list) and corresponding concentrations (phi_list) and resized concentration (phi_list_normalized). The starting concentration is printed at the end of integration to follow the progress of the search algorithm.

```
def Linewalk(phi0, h0, h_end, dh) : #walks a potential line
h = h0
phi = phi0
h_list = []#list of height values
phi_list = []#list of volume fraction values
phi_list_normalized = []#normalized list of volume fraction values
phi_end = 0
while(h >= 0 and h < h_end) : h_list.append(h)
phi_list.append(phi)
phi_list_normalized.append(phi/phi0)
step_dh = dh
k1 = direction(phi, h, B, labda)
k2 = direction(phi + 0.5 * dh * k1, h + 0.5 * dh, B, labda)
k3 = direction(phi + 0.5 * dh * k2, h + 0.5 * dh, B, labda)
k4 = direction(phi + dh * k3, h + dh, B, labda)
step_phi = (dh/6) * (k1 + 2 * k2 + 2 * k3 + k4)
while(phi + step_phi < 0 or step_phi > 10 * dh) : step_dh = step_dh/10
step_phi = step_phi/10
phi = phi + step_phi
h = h + step_dh
phi_end = phi
print(phi0)
return h_list, phi_list, phi_list_normalized, phi_end
```

This function uses the numerical integration function *Linewalk* to find the concentration profile that has the same number of particles as the experimental system. If one is only interested in finding the equilibrium concentration profile then this is the only function needed. The search algorithm used is very similar to simulated annealing except

for the difference that it searches to a given error instead of searching for a given number of steps. The inputs for this function are a guess starting concentration at a guess location and the length of the sedimentation vessel. The outputs are a list of distances and concentration, corresponding to the correct concentration profile. The print command prints the lists h_deflist and phi_deflist in a single list format for easy further data analysis.

```
def Find_curve(guess_phi, guess_h, concentration, length) :
concentration_try = 0
global h_def_list
global phi_def_list
h_def_list = []#list of height values
phi_def_list = []#list of volume fraction values
phi_def_list_normalized = []#normalized list of volume fraction values,
#change the return to _normalized to output normalizedend_phi = 0
dh = length/steps
b = 0
i = 0
increment = 0.25
if(concentration > 0.7405) : print('Error : Starting concentration is too high')
while(abs(concentration_try - concentration * length) > error) :
if concentration_try < concentration * length :
if b == 1 :
increment = 0.5 * increment
b = 0
while guess_phi + increment > 10000 :
increment = 0.9 * increment
guess_phi = guess_phi + increment
h_def_list, phi_def_list, phi_def_list_normalized, end_phi = Linewalk(guess_phi, guess_h, length, dh)
concentration_try = np.trapz(phi_def_list, x = h_def_list, dx = dh, axis = -1)
if concentration_try > concentration * length :
if b == 0 :
increment = 0.5 * increment
b = 1
while guess_phi - increment < 0 :
increment = 0.9 * increment
guess_phi = guess_phi - increment
h_def_list, phi_def_list, phi_def_list_normalized, end_phi = Linewalk(guess_phi, guess_h, length, dh)
concentration_try = np.trapz(phi_def_list, x = h_def_list, dx = dh, axis = -1)
if(increment < 10** - 30) : print('Error : Calculation failed, try lowering precisionor using more steps')
break

while i < len(phi_def_list) :
print(str(phi_def_list[i]) +' \t' + str(h_def_list[i]))
i = i + 1
return h_def_list, phi_def_list, guess_phi, end_phi
```

The function *Find_stationary_point* searches phi_def_list for a value within *error* of the initial concentration, thereby finding the, assumed, stationary point as described in the theory. As no interpolation method is used between the datapoints a large amount of steps is needed for time dependent analysis (more than 10000 is recommended.) The output is the ennumerator of the stationary point, which is the same for h_def_list and phi_def_list.

```
def Find_stationary_point(h_def_list, phi_def_list, starting_concentration :)
i = 0
n = 0
b = 0
check = 0
increment = int(len(phi_def_list))/2
while abs(phi_def_list[i] − starting_concentration) > error and check == 0 :
ifphi_def_list[i] > starting_concentration:
ifi + increment ≥ len(phi_def_list) : increment = int(increment ∗ 0.9)
ifb == 1 : increment = int(increment/2)
b == 0
i = i + increment
if phi_def_list[i] < starting_concentration:
ifi + increment < 0 : increment = int(increment ∗ 0.9)
ifb == 0 : increment = int(increment/2)
b == 1
i = i − increment
if increment == 0 : print('Could not meet precision, closest value
used.Error =' +str(phi_def_list[i] − starting_concentration))
check = 1
n = i
returnn
```

The function Force_stationary_point calculates the force on a single particle at the stationary point. The magnetic field of the rectangular bar magnet is used to calculate both the magnetic field and magnetic field gradient at the stationary point, where after the Langevin equation is used to find the force on a single independent particle. The inputs are the initial concentration ($c_0$) and the equilibrium concentration profile (*h_list* and *phi_list*). The output is a double corresponding to the force on a single particle in SI units. Note: make sure the same spacer distance is used for the equilibrium profile and time dependent calculations.

```
def Force_stationary_point(h_list, phi_list, c0) : n = Find_stationary_point(h_list, phi_list, c0)
h = h_list[n] + 1.84 * 10** - 3#additional factor for spacer
print('stationary points is at' + str(h_list[n]) +' meters')
force =
(((1/np. tanh((zeta * ((B/np.pi) * (np. arctan((L * W)/(2 * (h) * (4 * (h)**2 + L**2 + W**2)**0.5))
-np. arctan((L * W)/(2 * (R + (h)) * (4 * (R + (h))**2 + L**2 + W**2)**0.5)))))))-
(1/(zeta * ((B/np.pi) * (np. arctan((L * W)/(2 * (h) * (4 * h**2 + L**2 + W**2)**0.5))-
np. arctan((L * W)/(2 * (R + (h)) * (4 * (R + (h))**2 + L**2 + W**2)**0.5)))))))*
(labda * ((((2 * B * L * W)/np.pi) * ((((L**2 + W**2 + 8 * (h)**2)
/((L**2 + 4 * (h)**2) * (W**2 + 4 * (h)**2) * (L**2 + W**2 + 4 * (h)**2)**0.5))+
((L**2 + 8 * R**2 + W**2 + 16 * R * (h) + 8 * h**2)/((4 * R**2 + W**2+
8 * R * (h) + 4 * (h)**2) * (L**2 + 4 * (R + (h))**2)*
(L**2 + W**2 + 4 * (R + (h))**2)**0.5)))))) + (m * omega**2 * (h + mm_from_rotation_axis)))
print('Force in stationary point equals' + str(force))
return force
```

The function Find_delta_concentration finds $\Delta n$, the total concentration change between the equilibrium and initial concentration profiles. This is done by integrating the equilibrium profile from h=0 to h=stationary_point using the trapezium method and then subtracting initial concentration.

```
def Find_delta_concentration(h_list, phi_list, c0) : #check of deltaconcentration over hele lengte wel0is
n = Find_stationary_point(h_list, phi_list, c0)
height = h_list[n]
h_list = h_list[: n]
phi_list = phi_list[: n]
delta_c = (np.trapz(phi_list, h_list) - c0 * height)
print('Deltacequals' + str(delta_c) +' volume percent')
return delta_c
```

The function time_dependent_concentration calculates the initial speed of sedimentation by equating the friction and sedimentation forces. The friction factor is used. The option for the Batchelor correction for dipolar hard spheres is commented out, as it was found to be minor and needlessly complicated. The output is a plottable function and all the coefficients of Eq59, which is used for further data analysis.

```
def Time_dependent_sedimentation(height_coordinates, phi_coordinates, c_homogenous) :
h_def_list = np.linspace(0, height_coordinates[-1], steps * 10**3)
phi_def_list = np.interp(h_def_list, height_coordinates, phi_coordinates)
```

```
force = Force_stationary_point(h_def_list, phi_def_list, c_homogenous)
delta_c = Find_delta_concentration(h_def_list, phi_def_list, c_homogenous)
friction = (6 * np.pi * a * 0.0016)
batchelor_coefficient = 1
#if c_homogenous < 0.05 :
#Concentration — Dependent Sedimentation of Dilute MagneticFluids and Magnetic Silica Dispersions
#batchelor_coefficient = (1 − c_homogenous * (6.55 − 0.96 * ((mu * (4/3 * np.pi * (0.8 * a)**3
*magnetization)**2)**2/(32 * np.pi * k * T * a**3))))#klopt nog niet, controleren!
#else : #print('Volume fraction too high to use Batchelor approximation, usingStokes aprroximation')
#batchelor_coefficient = 1
time = np.arange(0.0, 14 * 3600 * 24, 1)
function = (np.exp(−(time * batchelor_coefficient * force * c_homogenous)/(friction*
delta_c))) * ((batchelor_coefficient * force * c_homogenous)/(friction))
print('Decay constant is' + str((force * c_homogenous
*batchelor_coefficient)/(friction * delta_c)))
print('Flux at t = 0equals' + str((force * c_homogenous * batchelor_coefficient)/(friction)))
print('Batchelor coefficient is' + str(batchelor_coefficient))
plt.plot(time, function)
plt.xlabel('time(days)')
plt.ylabel('total flux through stationary point(volume fraction * m/s)')
plt.title('time dependent sedimentation')
plt.show()
return function
```

In this section the actual function are being ran. In the current configuration a single equilibrium concentration profile is calculated and plotted.

```
#start_end_ratio = []#difference between concentration at h0 and h_end
#concentration = []
c = 0.0089
i = 1

#fig = plt.figure()
#fig.suptitle('No spacer iteration2', fontsize = 14, fontweight =' bold')
#ax = fig.add_subplot(111)
#fig.subplots_adjust(top = 0.85)
#ax.set_xlabel('Height[m]')
#ax.set_ylabel('Volume fraction[−]')

while(i < 2) : #Change_globals(1, 16)
ls1, ls2, phi0, phi_end = Find_curve(10** − 10 + c * 2, 0, c, 0.0165)
#Time_dependent_sedimentation(ls1, ls2, c)
#concentration.append(c)
#start_end_ratio.append(phi_end/phi0)
#print(phi_end/phi0)
```

```
plt.plot(ls1, ls2)
i = i + 1
plt.show()
```

# 10 Appendix B: Data analysis code

Note: the version of the data analysis code presented here is slightly outdated, as it contains several bugs in edge cases. The newest version of the code is present at the Physical & Colloid Chemistry group at Utrecht University.
This section of code converts the raw text datafile retrieved from the LumiFuge to a Mathematica 10 table object called "data". Within this object there are separate calleable objects, named and corresponding to xposition, time and transmission. In the end a 3D plot of these variables generated.

```
fileName = ''filepath''; << ''filepath\\LUMReader.m''
data = LUMData[fileName];

xposition = data[[All, 1]];
time = ToExpression[ToExpression[#]]&/@LUMTime[fileName][[2;;, 3]];
transmission = data[[All, 2;;]];
absorption = −Log10[(transmission − Min[transmission])/(Max[transmission] − Min[transmission])];
Do[Do[point[e][r] = {xposition[[e]], time[[r]], transmission[[e]][[r]]},
{e, 1, Length[xposition]}], {r, 1, Length[time]}];
Do[table[r] = Table[point[e][r], {e, 1, Length[xposition]}], {r, 1, Length[time]}];
alldata = Table[table[r], {r, 1, Length[time], 10}];
ListPointPlot3D[alldata, PlotRange → {Full, Full, Full}, PlotStyle → ''Rainbow'', AxesLabel
→ {''Height'', ''Time'', ''Transmission''}, ViewPoint → {Pi/2, −Pi, 1}, ImageSize → Large]
```

This section generates a table alldatarawabsorption, in which the transmission object is converted to absorption through the simple method as described in the thesis. The original large data table is shortened in by the third command. The first two numbers after $q$ determine ennumorators of xposition coordinates which will be included, the last number is determines how many timesteps are skipped between samples. Two plots are generated. The first plot is a 3D plot of the shortened rawabsorption table. The second plot is a plot of the po-

sition versus rawabsorption at the time given by the number within brackets after absorption.

```
Do[Do[point[q][w] = {xposition[[q]], time[[w]], absorption[[q]][[w]]}, {q, 1, Length[xposition]}], {w, 1, Length[time]}];
Do[table[q] = Table[point[q][w], {w, 1, Length[time]}], {q, 1, Length[xposition]}];
alldatarawabsorption = Table[table[q], {q, 600, 1750, 15}];
ListPointPlot3D[alldatarawabsorption, PlotStyle->``Rainbow'',
AxesLabel → {``Height'', ``Time'', ``Concentration''}, ViewPoint → {Pi/2, 1.5, 1}, ImageSize → Large]
ListPlot[{Transpose[{xposition, absorption[[All, -1]]}], Transpose[{xposition, absorption[[All, 200]]}]},
PlotRange → Full, AxesLabel → {``Distance from rotation axes [mm]'', ``Volume fraction [-]''},
ImageSize → Large, PlotMarkers->{``◆'', 5}]
```

This section of code is equivalent to the previous section except for the replacement of the rawabsorption object by the normalized absorption object. All absorption values at location $i$ are normalized in the same way so that the the absorption at $t = 2$ are equal to initialc. This method gets rid of optical broadening at the edge of the magnet and static noise from nicks and grease on the sedimentation vessel. For optimal performance it is recommended to take a lot of measurements in the first minute and normalize on the average. This method is invalid if the assumption that the initial suspension is homogenous is false, or if there is significant optical saturation.

```
initialc = 0.01685;

Do[absorption[[i, All]] = absorption[[i, All]] * (initialc/(absorption[[i, 2]])), {i, Length[transmission[[All, 0]]]}];
Do[Do[point[q][w] = {xposition[[q]], time[[w]], absorption[[q]][[w]]}, {q, 1, Length[xposition]}], {w, 1, Length[time]}];
Do[table[q] = Table[point[q][w], {w, 1, Length[time]}], {q, 1, Length[xposition]}];
alldata = Table[table[q], {q, 600, 1750, 15}];
ListPointPlot3D[alldata, PlotStyle->``Rainbow'', AxesLabel → {``Height'', ``Time'',
``Concentration''}, ViewPoint → {Pi/2, 1.5, 1}, ImageSize → Large]
ListPlot[{Transpose[{xposition, absorption[[All, -1]]}], Transpose[{xposition, absorption[[All, 200]]}]},
PlotRange → Full, AxesLabel → {``Distance from rotation axes [mm]'', ``Volume fraction [-]''},
ImageSize → Large, PlotMarkers->{``◆'', 5}]
```

This section checks if the integrated absorption over a range of spatial coordinates at the initial time and final time are equal. The output is the percentage of deviation between the two integrations. If the final integrated absorption is significantly lower than the initial integrated absorption this indicates that there is optical saturation in the final concentration profile. When there is less integrated absorption at the inital time there is optical saturation in the initial concentration profile.

```
Δvolumebegineind =
(Integrate[Interpolation[Transpose[{xposition, absorption[[All, -1]]}], InterpolationOrder → 2][x], {x, 107, 124.5}]-

Integrate[Interpolation[Transpose[{xposition, absorption[[All, 1]]}], InterpolationOrder → 2][x], {x, 107, 124.5}])/
Integrate[Interpolation[Transpose[{xposition, absorption[[All, 1]]}], InterpolationOrder → 2][x], {x, 115, 116}]
```

This section plots the average concentration as function of time for the interval $x, x_0, x_{end}$. This is used for the comparison of the time dependent theory.

```
(*Plots the average concentration in the interval{x, x_0, x_end}as function of time*)
change = Table[Integrate[Interpolation[Transpose
[{xposition, absorption[[All, i]]}], InterpolationOrder → 1][x], {x, 124, 110}], {i, Length[time]}];
ListPlot[Transpose[{time, change/(124 - 110)}]]
```

# References


[1] R. E. Rosensweig. Ferrohydrodynamics. Courier Corporation., 1985.

[2] Laura L. Vatta. Floating diamonds with nanomagnetic particles. Macromolecular Symposia, 225:221–228, 2005.

[3] E. J. Bakker, P. C. Rem, and N. Fraunholcz. Upgrading mixed polyolefin waste with magnetic density separation. Waste Management, 29(5):1712–1717, 2009.

[4] Susamu Taketome. Motion of Ferrite Particles under a High Gradient Magnetic Field in a Magnetic Fluid Shaft Seal. Japanese journal of applied physics, 19(10):1929–1936, 1980.

[5] R.E. E Rosensweig. Magnetic Fluids. Scientific American, 247(4):136–145, 1982.

[6] J. F. Berret, O. Sandre, and A. Mauger. Size distribution of superparamagnetic particles determined by magnetic sedimentation. Langmuir, 23(6):2993–2999, 2007.

[7] Randall M. Erb, David S. Sebba, Anne A. Lazarides, and Benjamin B. Yellen. Magnetic field induced concentration gradients in magnetic nanoparticle suspensions: Theory and experiment. Journal of Applied Physics, 103(6), 2008.

[8] Charles Kittel. Introduction to Solid State Physics. 2010.

[9] C. Kittel. Elementary Statistical Physics, volume 27. 1959.

[10] E.M. Lifshitz and L.D. Landau. Statistical Physics. Pergamon Press, 3rd edition, 1959.

[11] F. Penna and P. Tarazona. Dynamic density functional theory for steady currents: Application to colloidal particles in narrow channels. Journal of Chemical Physics, 119(3):1766–1776, 2003.

[12] Dirk Gillespie, Wolfgang Nonner, and Robert S Eisenberg. Coupling PoissonNernstPlanck and density functional theory to

calculate ion flux. Journal of Physics: Condensed Matter, 14(46):12129–12145, 2002.

[13] Randall M. Erb and Benjamin B. Yellen. Concentration gradients in mixed magnetic and nonmagnetic colloidal suspensions. Journal of Applied Physics, 103(7):2006–2009, 2008.

[14] Albert P. Philipse. Remarks on the Donnan condenser in the sedimentation-diffusion equilibrium of charged colloids. Journal of Physics Condensed Matter, 16(38):4051–4062, 2004.

[15] Eric W. Weisstein. Sphere packing. page http://mathworld.wolfram.com/SpherePacking.html. Wolfram Research, Inc., 1999.

[16] Norman F. Carnahan and Kenneth E. Starling. Equation of state for nonattracting rigid spheres. The Journal of Chemical Physics, 51(2):635–636, 1969.

[17] Eric W. Weisstein. Lambert W-Function. Wolfram Research, Inc.

[18] Endri Süli and David Mayers. An Introduction to Numerical Analysis. Number 1. 2003.

[19] Ekaterina A. Elfimova, Alexey O. Ivanov, and Philip J. Camp. Thermodynamics of ferrofluids in applied magnetic fields. Physical Review E - Statistical, Nonlinear, and Soft Matter Physics, 88(4):1–11, 2013.

[20] Hiroshi Fujita. Mathematical Theory of Sedimentation Analysis. 1962.

[21] W. B. Russel, D. A. Saville, and W. R. Schowalter. Colloidal Dispersions. 1992.

[22] Bob Luigjes, Dominique M E Thies-Weesie, Ben H. Erné, and Albert P. Philipse. Sedimentation equilibria of ferrofluids: II. Experimental osmotic equations of state of magnetite colloids. Journal of Physics Condensed Matter, 24(24), 2012.

[23] Bob Luigjes, Dominique M.E. Thies-Weesie, Albert P. Philipse, and Ben H. Erné. Sedimentation equilibria of ferrofluids: I. Analytical centrifugation in ultrathin glass capillaries. Journal of Physics Condensed Matter, 24(24), 2012.

[24] Roberto Piazza, Tommaso Bellini, and Vittorio Degiorgio. Equilibrium Sedimentation Profiles of Screened Charged Colloids: A Test of the Hard-Sphere Equation of State. Physical Review Letters, 71(25):4267–4270, 1993.

[25] Liesbeth N Donselaar, Albert P Philipse, and Jacques Suurmond. Concentration-Dependent Sedimentation of Dilute Magnetic Fluids and Magnetic Silica Dispersions. Langmuir, 13(23):6018–6025, 1997.

[26] Mark Klokkenburg, Ben H. Erné, Johannes D. Meeldijk, Albrecht Wiedenmann, Andrei V. Petukhov, Roel P.A. Dullens, and Albert P. Philipse. In situ imaging of field-induced hexagonal columns in magnetite ferrofluids. Physical Review Letters, 97(18):4–7, 2006.

[27] Jongnam Park, Kwangjin An, Yosun Hwang, J. E.Geun Park, Han Jin Noh, Jae Young Kim, Jae Hoon Park, Nong Moon Hwang, and Taeghwan Hyeon. Ultra-large-scale syntheses of monodisperse nanocrystals. Nature Materials, 3(12):891–895, 2004.

[28] B Luigjes, S M C Woudenberg, R De Groot, J D Meeldijk, and H M Torres Galvis. Diverging Geometric and Magnetic Size Distributions of Colloidal Iron Oxide Nanocrystals. The journal of phyisical chemistry C, page 2064, 2011.

[29] Réne Massart. Preparation of aqueous magnetic liquids in alkaline and acidic media. IEEE Transactions on Magnetics, 17(2):1247–1248, 1981.

[30] S. Lefebure, E. Dubois, V. Cabuil, S. Neveu, and R. Massart. Monodisperse magnetic nanoparticles: Preparation and dispersion in water and oils. Journal of Materials Research, 13(10):2975–2981, 1998.

[31] R.W. Chantrell, J. Popplewell, and Stuart.W. Charles. Measurements of particle size distribution parameters in ferrofluids. Magnetics, IEEE Transactions on, 14(5):975–977, 1978.

[32] Jos Van Rijssel, Bonny W M Kuipers, and Ben H Erné. Non-regularized inversion method from light scattering applied to ferrofluid magnetization curves for magnetic size distribution analysis. Journal of Magnetism and Magnetic Materials, 353:110–115, 2014.

[33] R. Engel-Herbert and T. Hesjedal. Calculation of the magnetic stray field of a uniaxial magnetic domain. Journal of Applied Physics, 97(7):8–12, 2005.

[34] F. A. Gonçalves, K. Hamano, and J. V. Sengers. Density and viscosity of tetralin and trans-decalin. International Journal of Thermophysics, 10(4):845–856, 1989.